DLR AT-TRA
IB 92517-15 B7

JExTRA – Jet Noise Experiments at AT-TRA

SUMMER 2015 PROJECT REPORT

Max Nussbaumer and Henri Siller

Deutsches Zentrum für Luft- und Raumfahrt e.V.
Institut für Antriebstechnik
Abteilung Triebwerksakustik
Berlin

DLR **Deutsches Zentrum für Luft- und Raumfahrt**

Deutsches Zentrum für Luft- und Raumfahrt e.V.
Institut für Antriebstechnik
Abteilung Triebwerksakustik
Prof. Dr. Lars Enghardt
Müller-Breslau-Straße 8
10623 Berlin
Tel: +49 30 310006-18

Max Nussbaumer and Henri Siller
Tel: +49 30 310006-(030) 310 006 -57
Fax: +49 30 310006–39
E-Mail: Henri.Siller@dlr.de

Dokument-Identifikation

Titel	JExTRA – Jet Noise Experiments at AT-TRA
Thema	DLR AT-TRA
Autor(en)	Max Nussbaumer and Henri Siller
Dateiname	IB92517_15BX_JEXTRA.tex
Zuletzt gespeichert am . .	12. Januar 2016

Dokument-Entwicklung:

Version 1.0	inital version	January 12, 2016

Inhaltsverzeichnis

1. Abstract

Dieser Bericht wurde von Max Nussbaumer im Rahmen seines Praktikums in der DLR Abteilung Triebwerksakustik in Berlin vom 1. Juli 2015 bis zum 11. September 2015 geschrieben. Betreut von Henri Siller hat er akustische Messungen an dem JExTRA Strahlprüfstand mit einem Mikrofonarray durchgeführt. Der Strahlprüfstand wurde von Robert Meyer bereitgestellt, der reflexionsarm Aufbau von Alessandro Bassetti konzipiert und aufgebaut. Unterstützt wurde er von von Wolfram Hage und Larisa Hritsevskyy, die zusammen mit Stefan Funke an den Messungen beteiligt waren. Stefan Funke hat bei der Auswertung der Daten beraten und Karsten Liesner unterstützte den Betrieb des Prüfstands und Anpassungen der Steuersoftware.

This report by Max Nussbaumer is the result of his summer internship from 1. July 2015 to 11. September 2015 at DLR engine acoustics in Berlin. Under the supervision of Henri Siller, he performed acoustic measurements with a microphone array in the JExTRA jet facility. The jet facility was provided by Robert Meyer, the anechoic set-up of the microphone array has been conceived and constructed by Alessandro Bassetti with the support of Wolfram Hage and Larisa Hritsevskyy, who together with Stefan Funke supported the experiments. Stefan Funke also consulted Max Nussbaumer during the data reduction. Karsten Liesner supported the operation of the jet facility and adapted the control software.

2. Introduction

The JEXTRA project concerns the establishment of a small scale jet noise testing facility at the DLR Berlin Charlottenburg Location.

This report covers the work carried out on the project from 1. July 2015 to 11. September 2015.

In the firs phase of the project, the partially complete JEXTRA rig was brought to a state in which it can be used for measurements. The practical steps taken are documented in chapter 3.

In the second phase of the project the capabilities and limitations of the JEXTRA rig were investigated in a series of tests. Experiments with single sound sources to identify reflecti ons are covered in chapter 5, Jet noise measurements are covered in chapter 6. As part of this phase of the project a new microphone calibration script was developed in python, the mathematical background, methodology and implementation of this script are covered in chapter 4. Recommendations for future work on the JEXTRA project are given in chapter 7.

3. Design and Set-up of Rig

3.1. Linear Array Design

In order to carry out source identification the construction of a linear array for use in the anechoic channel around the jet is desired. The SODIX method will be used to interpret the data from this linear array. The necessary length, microphone spacing and number of microphones to be used need to be determined. There is no define minimum spatial microphone spacing for the SODIX method [Stephan], although some evidence of an aliasing-like effect at high frequencies has been observed. In general however, for SODIX, the more data points are available the better the results from the optimisation.

In order to allow some of the data to be used for an alternative beam-forming technique, the minimum spacing as required for beam-forming will be calculated for the 60° to 100° region and applied to the entire array. Sections of the array outside this range may not be suitable for beam-forming above a certain frequency, but should still be able to be used with SODIX.

3.1.1. Microphone spacing

The microphones initially intended to be used are assumed to be approximately linear up to 16 kHz, so this is taken as the maximum frequency of interest f_{max}.

The minimum spatial sampling rate for microphones in a linear array, to avoid aliasing when using beam-forming methods, is half the smallest wavelength of interest. The relevant wavelength for this is the 'trace wavelength' (λ_t*) as seen by the microphones [Stephan]. The smallest trace wavelength will occur at the angle furthest from 90°. In this set-up this is the 60° angle, as below 60° there is no requirement for beam-forming to be applicable.*

The definitio of λ_t is shown in figur 3.1. As the wavelength at 16 kHz is $\lambda = 21.14\,mm$ (see below), the closest microphone is around 27 wavelengths away from the sound source, which justifie the plane wave assumption.

Abbildung 3.1.: **Definitio of λ_t for a polar angle of θ.**

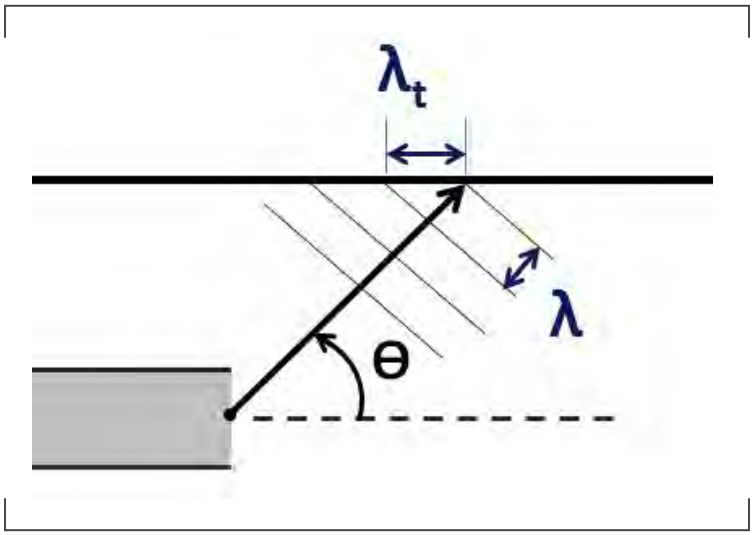

First the minimum wavelength λ_{min} must be calculated. This is given by $\lambda_{min} = a / f_{max}$ where a is the speed of sound. Taking the temperature of air as 25 °C, and using standard values for R and γ of air, a can be calculated as:

$$a = \sqrt{\gamma * R * T_{static}}$$

$$a = \sqrt{1.4 * 287 * (273.15 + 20)} = 343\,m/s$$

thus:

$$\lambda_{min} = 343/16000 = 0.02144\,m = 21.14\,mm$$

Simple trigonometry can then be applied to work out λ_t:

$$\lambda_t = \frac{\lambda}{\cos(60)} = 2\lambda$$

then to find the minimum spatial sampling rate d:

$$d < [\lambda_t]_{min}/2$$

thus $d < 21.14\,mm$

The temperatures of the jet and the surrounding air are likely to rise during operation. This will increase the speed of sound and thus increase λ_{min}*. This means that the coldest operating temperature is the critical condition. For example, repeating the above calculation with an air temperature of 25 °C gives* $d < 21.63\,mm$ *.*

In summary, to avoid beam-forming aliasing at 16 kHz, in the range 100° to 60° the minimum spacing required is 21 mm.

3.1.2. Length of Array

The length of the array depends on the range of polar angles that are of interest. In the field of pure jet noise, 'observation angles' or 'polar angles' are defined from the positive jet axis (i.e. the direction of the jet) (see figure 3.2).

Abbildung 3.2.: **Definition of observer angle θ in jet noise aeroacoustics.**

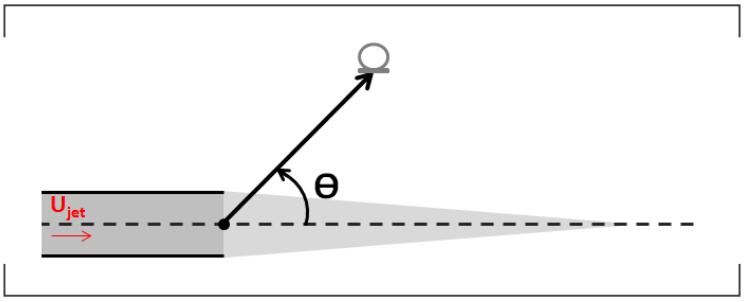

By translating the linear array (or whole anechoic channel) in the axial direction, it is possible to alter the polar angles of the microphones as shown in figure 3.3.

The axial translation of the anechoic channel is limited by geometric constraints due to a construction above the pipe as shown in figure 3.4. The distance marked s in the sketch is the distance between the frame constraint and the nozzle, this distance can be extended to a maximum approximately $s \approx 270\,mm$ by moving some elements of the construction. If this is less than the required length then either the pipe needs to be lengthened, or the

Abbildung 3.3.: **Maximum (firs microphone) and minimum (last microphone) polar angles measured for a given axial position of the anechoic channel and linear array relative to the nozzle exit.**

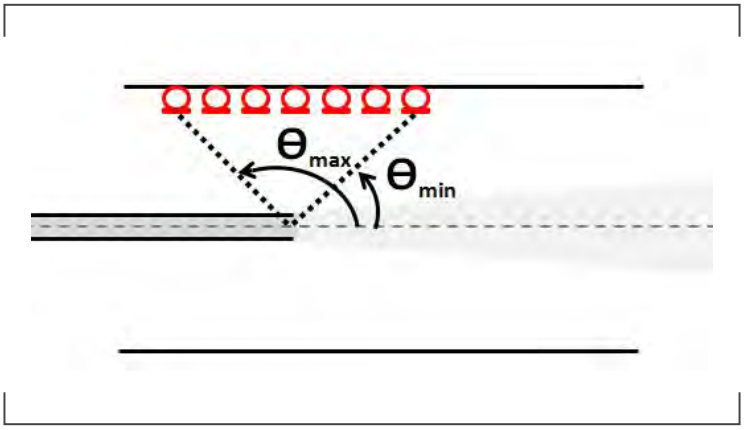

range of observer angles reduced. Taking into account the fact that for effective sound insulation, microphones should not be installed too close to the entrance of the channel, it has been decided to reduce the largest observer angle of interest from 120° to 100°.

Abbildung 3.4.: **Geometric constraint of anechoic channel translation. Critical location marked in orange.**

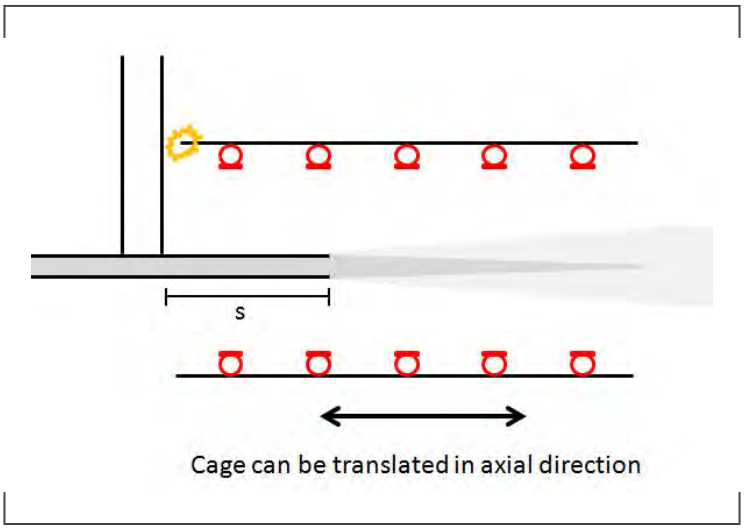

Downstream of the jet, results from another project have shown that microphones at angles lower than 50° may give interesting results [Jonas]. In order to obtain data for this region the fina range of observer angles has been specifie as 30° – 100°.

In order to calculate the length of array needed it is firs necessary to consider the radial distance between the jet axis and the microphones. The inner layer of sound insulation

starts at 0.7 m from the jet axis. In order to avoid interference by possible reflection from the sound-absorbing material it has been proposed [Henri] that the microphones are placed as far form the wall as possible. With the proposed linear array design a radial distance of 580 mm between the microphone heads and the jet axis can be achieved.

For the range of polar angles specifie (30°- 100°) the following lengths are needed upstream and downstream of the nozzle exit:

$$l_{upstream} = 0.580 * \tan 10 = 102.3\, mm$$

$$l_{downstream} = 0.580 \ / \tan 30 = 1004.6\, mm$$

(For comparison the length of one channel element is ≃ 490 mm, so the array will have to extend over three elements.)

A microphone spacing of 20.9 mm has been chosen as this will allow a symmetrical segment to be used for each panel [Wolfram]. Each of these linear array segments will consist of 22 microphone possible positions.

The number of microphones needed for this length of array is roughly 52, with 46 microphones downstream, and 5 microphones upstream of the microphone directly at the nozzle exit. For practical reasons the number of microphones has been reduced to 50 (44 downstream). With eight breakout boxes (see source [22]) giving 64 channels, this allows 12 channels to be used for microphones on a ring and 2 channels to be free for purposes such as detection of microphone positions (see appendix D) Using 50 microphones in the linear array still allows an angle of 30.6° to be obtained, which is considered close enough to the suggested 30°.

In order to avoid the effects of reflection at the channel entrance, the microphones are to be placed as far downstream as possible, with the nozzle exit extending into the anechoic channel. This is limited by the geometric constraint, characterised by the length $s = 270\, mm$*. Thus the microphone directly under the nozzle exit can only be 270 mm from the channel entrance. This allows for the required fiv microphones upstream of the zero position, with the firs microphone in the array then being roughly 165 mm from the channel entrance.*

The design of the channel means that it is not possible to avoid gaps between the segments of the linear array on adjacent panels. The spacing between the microphones on either side of this gap is $490 - (21 * 20.9) = 51.1$ *mm.*

The distribution of the microphones will be such that 16 microphone positions on the firs element, 22 on the second and 12 on the third element will be used. A benefi of the array design is that it can easily be reused for application where a different number of microphones is required (such as if a different range of polar angles is specified)

Figure 3.5 shows the polar angles of the different microphone positions against their axial coordinate downstream from the nozzle exit.

Abbildung 3.5.: **Polar angle versus axial position of microphone for a dead-centre jet position, and microphones at 580 mm from the centre. Microphone positions to be used marked in blue.**

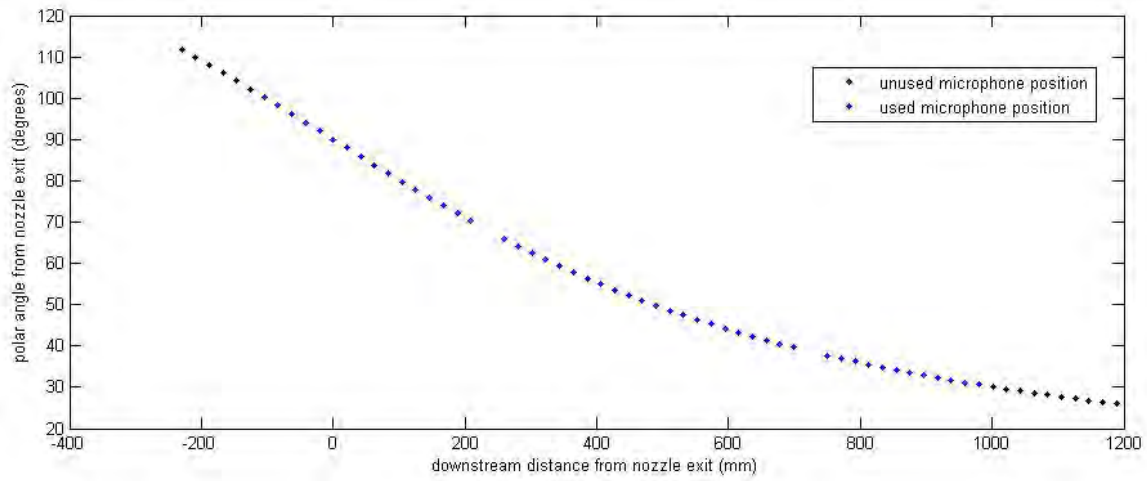

3.1.3. Design and Construction

Based on the above recommendations, a linear array consisting of an aluminium holding element and brass tubes has been designed [Wolfram] and built in the metal workshop. Upon installation of the linear array it has become apparent that imperfections in the brass tubes (light bends etc.) mean that the positions of the microphones deviate by a

few mm from there nominal values. It needs to be investigated whether the deviations fall within the acceptable range, and whether there are methods of precisely determining the position of the microphones (see appendix D).

Abbildung 3.6.: **CAD model of Linear Array in position on Anechoic Channel. Channel elements are labelled A-E. Jet direction is indicated by the arrow labelled U_{jet}**

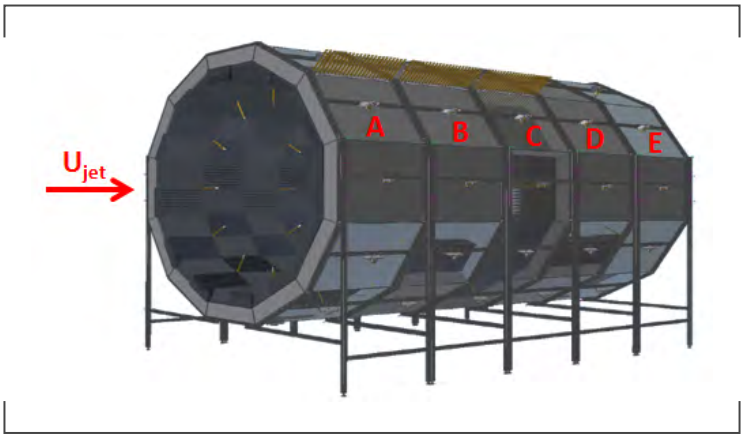

Figure 3.6 shows a CAD model of the linear array attached to the anechoic channel. Note that, in the actual construction, the position of the linear array has been rotated by 15° clockwise with respect to the original CAD model for ease of access. Refer to further CAD drawings for more details of the design [Wolfram Hage]. Figure 3.7 shows a photograph of the installed linear array viewed from the exit of the anechoic channel.

3.1.4. Conclusions for Linear Array Design

-To avoid aliasing for beam-forming up to a frequency of 16 kHz and over a polar angle range 60° to 100°, a microphone spacing of under 21 mm is required (calculated using λ_t).

-The length of an array needed to achieve polar angles in the range 30° to 100° is such that linear array segments need to span across three elements of the anechoic channel.

-A linear array consisting of three segments, each with 22 microphone positions at spacings of 20.9 mm has been designed and constructed.

Abbildung 3.7.: **Photographs of the installed linear array, taken during Single Source Tests 20/08/15**

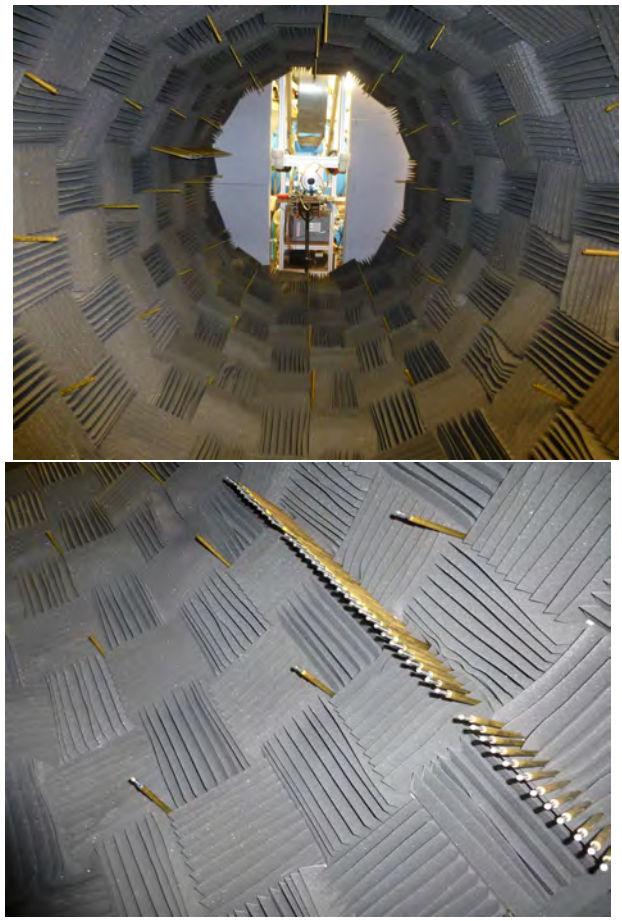

-For the current scenario, the array would require 50 microphones, spaced at 20.9 mm with two 51.5 mm gaps between elements where no microphones can be positioned.

-The true microphone positions deviate slightly from their nominal values. A method for determining their true positions to a sufficien degree of accuracy remains to be developed (appendix D).

3.2. Low-Reflectio Rear and Front Wall for Anechoic channel

Although the jet itself is in a low-reflectio channel, reflection from the two open ends may still affect the microphone measurements as can be seen in figur 3.2.

Abbildung 3.8.: **Sketch of reflection of sound waves from equipment at front and wall at rear. (Not to Scale)**

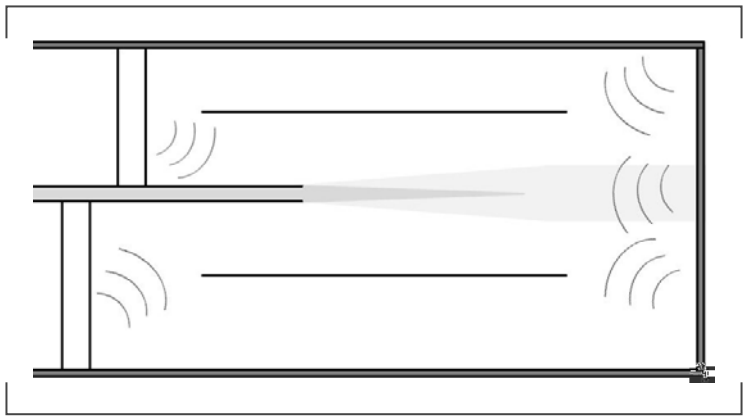

The two ends cannot be completely blocked off because a flo of entrained air through the tube needs to be enabled. Limiting this flo of air will result in a jet whose structure is not representative of a free-stream jet. The materials used to construct the anechoic channel are porous, but do not allow for sufficien airflo to sustain the entrainment of air by the jet.

Thus air will flo in through the entrance of the anechoic channel, and will flo out of the far end of the anechoic channel together with the air from the jet as shown in figur 3.2. It is important to have an idea of what kind of mass flow and velocities we are expecting in order to design the low-reflectio components for the front and rear of the tube to block off reflection from the equipment and rear wall, without impeding the airflo too much. Measurements of the airspeed using a 'flugelrad anemometer showed that the flo of air into the front of the channel is small, suggesting that a front-wall construction will not have too great an effect on the jet characteristics.

A simple design consisting of a 2 m by 2 m wall of BASOTECT sown onto a perforated sheet and attached to the cupboards at the back of the room, accompanied by two 50 cm by 1 m panels hanging at the front is envisioned. More details on the construction of these low-reflectio 'walls' can be found in section 3.4.2.

Abbildung 3.9.: **Sketch of entrainment of ambient flo by jet. (Not to Scale)**

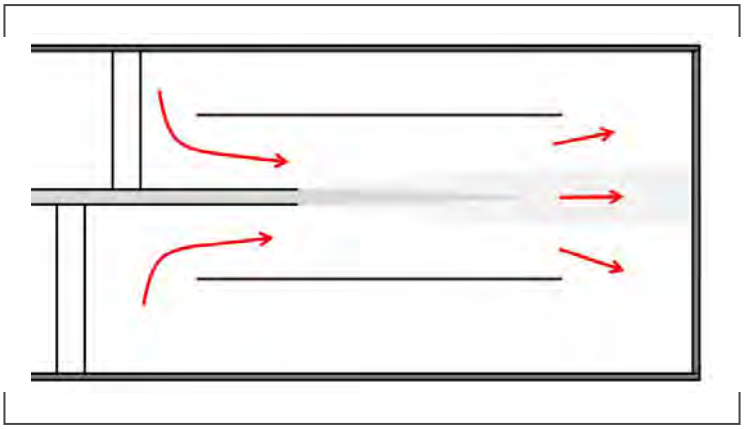

Abbildung 3.10.: **Sketch of entrainment of ambient flo by jet, with possible low-reflectio components coloured in blue. (Not to Scale)**

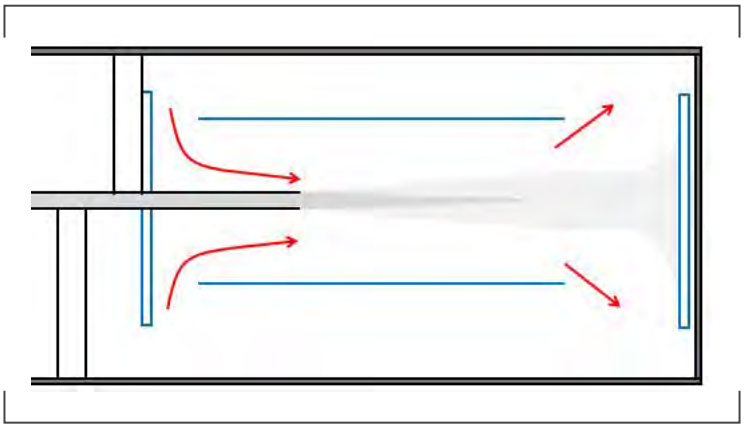

3.3. Positioning of the Anechoic Channel and Microphones

The segments of the anechoic channel are connected into two blocks. Segments A, B and C make up the firs block, which holds the linear array and is to be precisely positioned, while segments D and E make up the second block which can be moved to allow access to the microphones in block ABC.

The accurate positioning of the channel is a time consuming process, and ideally block ABC should remain in position so that this does not have to be carried out. However, all of the positioning procedures used were chosen for their repeatability. By following the steps described in this section it should be possible to accurately reassemble and position block ABC if for some reason it has had to be disconnected and/or moved. Figure 3.11 shows the coordinate system used throughout this document.

Abbildung 3.11.: **Coordinate system used.**

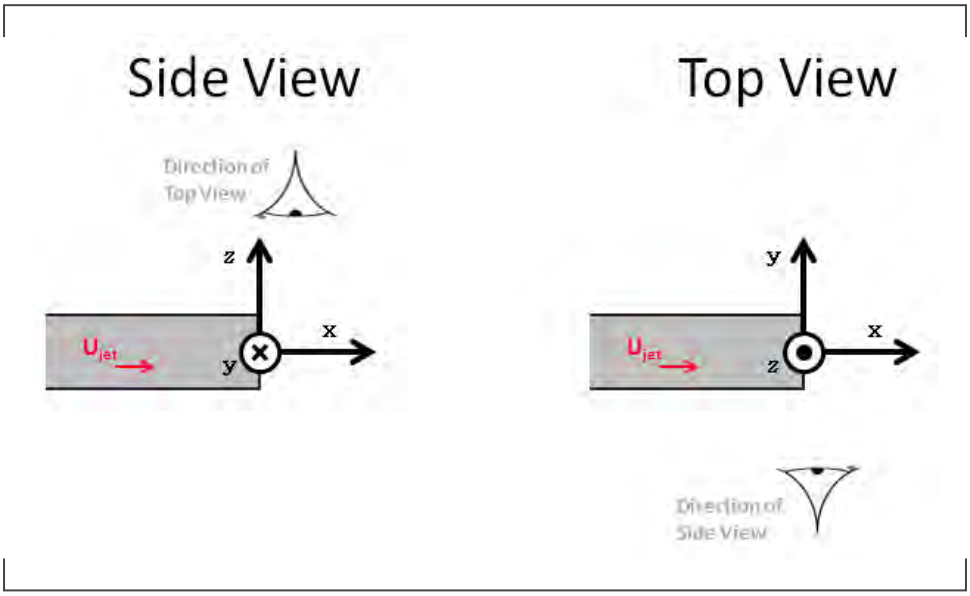

3.3.1. Markings on Channel Segments and Room

Figure 3.12 shows markings made on the individual segments of the channel. These can be used to adjust the segments into the correct shapes by ensuring the dimensions are as noted in the sketch, and the lines on adjacent sections line up.

Figure 3.13 shows the markings made on the walls. All of these are carefully positioned with respect to the jet axis. There is a line mirroring the jet axis drawn on the ceiling. On the floo , there is a line mirroring the jet axis near the nozzle, while further downstream there are two lines parallel to the jet axis, but translated by 26 cm to either side.

3.3.2. Positioning in X-Y plane

In order to position the channel, plumb lines are descended from block ABC: one at the front and two at the rear. The string is attached using screws in sliding blocks with notched plates which the string can hook into. Alternatively the string can be wrapped around the screw and tied in place. The plumb lines are positioned such that the string is hanging down exactly from the relevant markings on the element and the plumb line tip

Abbildung 3.12.: **Segment markings. Not to scale.**

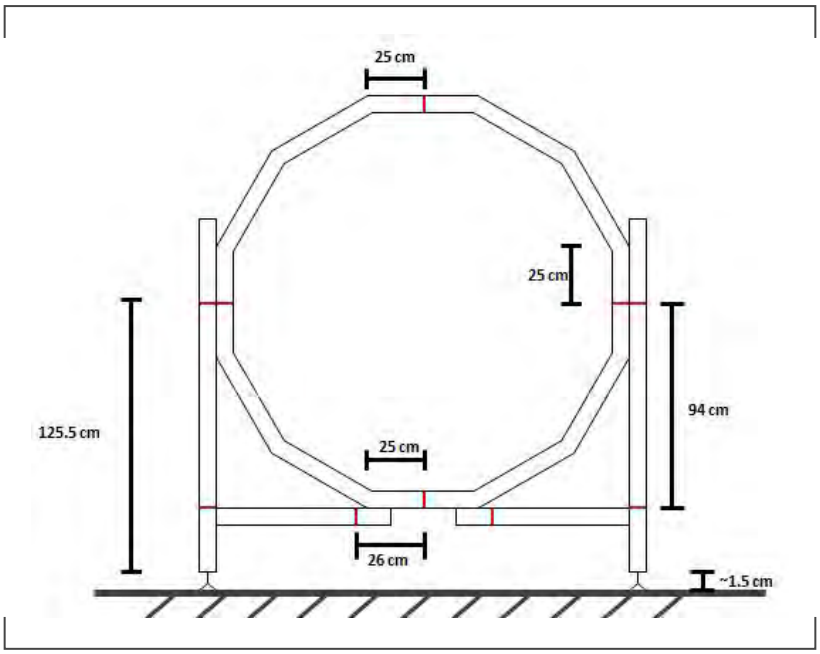

is as close as possible to the ground without actually making contact.

Figure 3.14 shows the plumb line positions on the front and rear of block ABC. The wire connection to the ceiling is also shown. The ceiling connections are only attached when the horizontal position has been set to a firs degree of accuracy. The suspension from the ceiling is required to make the channel more regular in shape and help with the vertical positioning.

*The three plumb lines should be accurately positioned on the lines marked on the floo in order to set the position in the y-direction. For the x-direction (i.e. axial) the current position is marked with an arrow pointing to the position along the front line on the floo onto which the front plumb line should descend. The word '*hier*' is written next to this arrow for clarification Note that this position could be changed to control the polar angles of the microphones if required.*

3.3.3. Positioning in Z-direction

Once the position in the x-y plane has been set, the vertical position of the channel needs to be altered in order to ensure that the jet axis is central. In order to do this, a temporary construction representing the jet axis is used (see figur 3.18 in section 3.4.1).

Abbildung 3.13.: **Side view of markings on walls (in red). Arrows indicate where plumb lines are used for positioning of elements. Temporary construction to represent jet axis and help with vertical alignment is shown in light grey. Not to scale.**

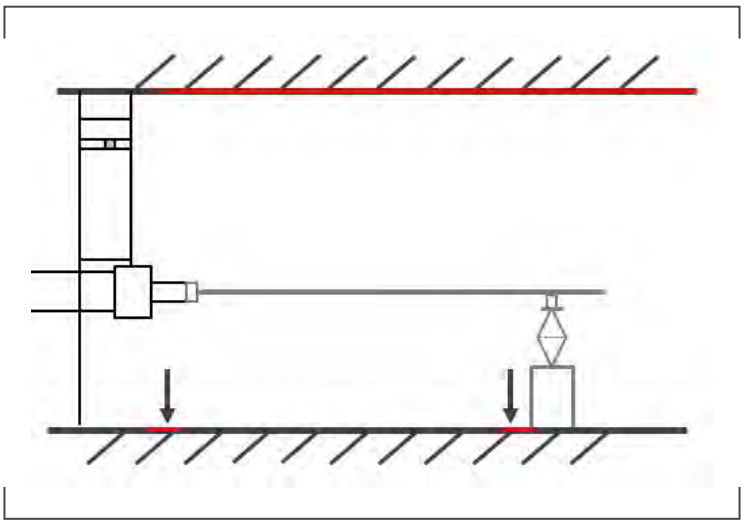

The temporary construction is adjusted and positioned using plumb lines and a spirit level (Wasserwaage). Block ABC is adjusted so that its centre coincides with the jet axis, by adjusting the length of the feet (bottom) and using the rigging (Wantenspanner) to pull up the top. Figure 3.15 gives a side view of the attachment to the ceiling, and the temporary construction representing the jet axis.

3.3.4. Positioning of Microphones

Figures 3.16 and 3.17, show the distance from the jet-axis of the microphones in the linear array and ring respectively. The temporary jet-axis pipe construction can be used to check these dimensions. Unfortunately this is not as accurate as desirable. Ultimately it will not be possible to position microphones to a high accuracy. It is therefore important that the exact positions of the microphones are known (see appendix D).

3.4. Practical Protocol

This section gives a brief overview of the practical steps taken to set up the jet-noise rig.

Abbildung 3.14.: **Front (left) and Rear (right) view of element ABC, with plumb line positions indicated by arrows. Not to scale.**

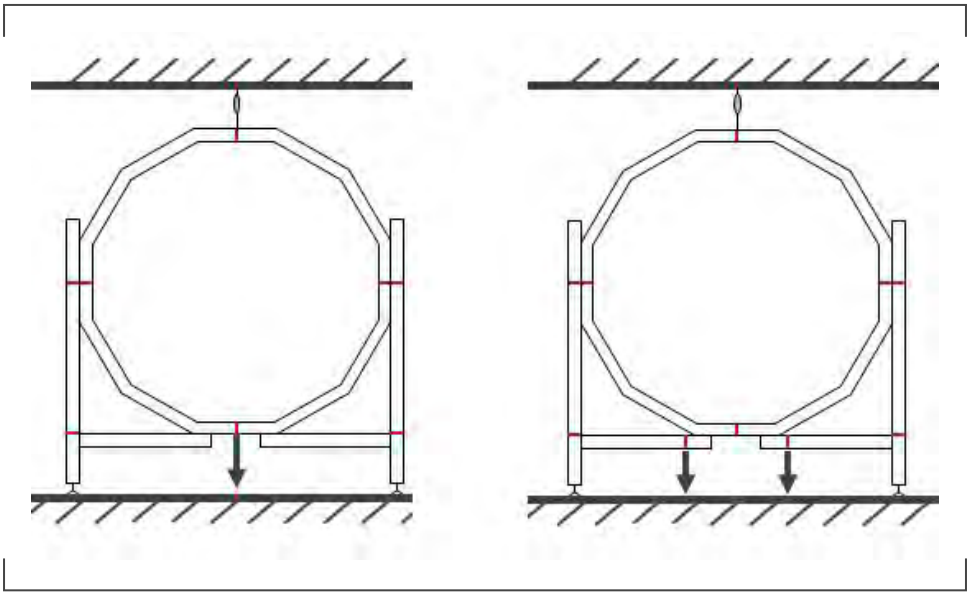

3.4.1. Theme: Anechoic Channel

Task: Adjustment of Height and Shape of Channel

Details*: Five rings, constructed out of aluminium elements, with two 10 cm layers of sound insulation (BASOTECT and acoustic wedge foam)*

Subtask*: Adjust height of rings to ensure jet is positioned centrally. Adjust shape of rings to ensure that these are of a regular shape. Adjustments need to be done with segments lying on floo . (see section 3.3 for numerical adjustments made)*

Subtask*: Suspension from ceiling using steel rope, hook screws and rigging (Wanten-spanner) -this ensures that despite the low rigidity of the segments these are still roughly regular in shape and not oval. Holes drilled into the ceiling are positioned above the jet centre line (positioned using plumb lines).*

Abbildung 3.15.: **Sketch of room showing wall markings, temporary jet axis set-up and wire ceiling connections for element ABC. Channel segments are in dotted lines. Not to scale.**

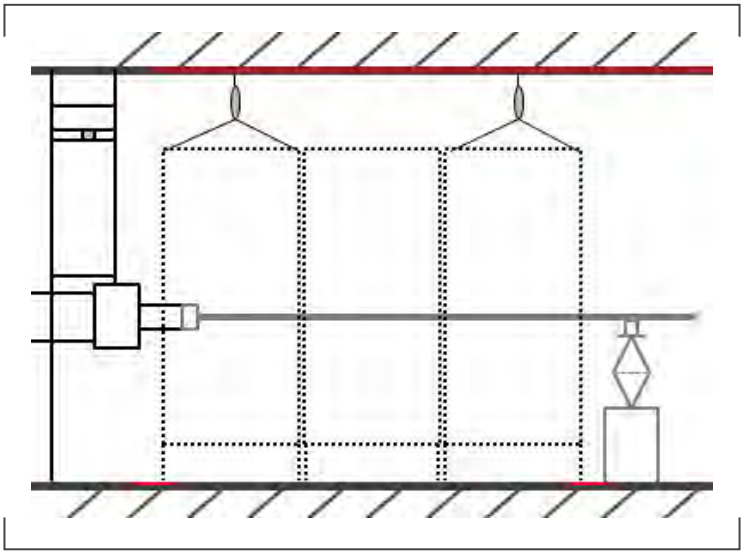

Task: Assembly and Positioning

Subtask*: Connect segments A,B,C and D,E together at 14 positions using tabs (German: Laschen) to form two blocks.*

Subtask*: Horizontal Positioning of block ABC using 3 plumb lines (German: Lot) and line markings on the floo (N.B. the floo markings were partially constructed with help of the precisely positioned traverse situated under the jet). At least two, and preferably three people are needed for this positioning.*

Subtask*: Vertical Positioning of block ABC by setting up a tube to represent the jet axis. This tube is attached to the nozzle (using a specially constructed aluminium nozzle plug with a centrally positioned hole for the tube) and a stand (with a screw-jack for adjusting height) on the downstream side. The stand (shown in figur 3.18) is positioned by plumb lines and a spirit level tool (German: Wasserwaage). Measurements to the top and bottom of the rings are used to position the block vertically, ensuring that the jet axis is centrally positioned. The vertical adjustment is carried out by changing the length of the feet (bottom) and the suspension wire (top) (using rigging (German: Wantenspanner)).*

Subtask*: Attach block DE to block ABC using 14 connectors. Ensure block ABC does not move from its set position. Attach ceiling suspension to segment E and adjust to correct*

Abbildung 3.16.: **Positioning of Linear array microphones with respect to jet axis. Not to scale.**

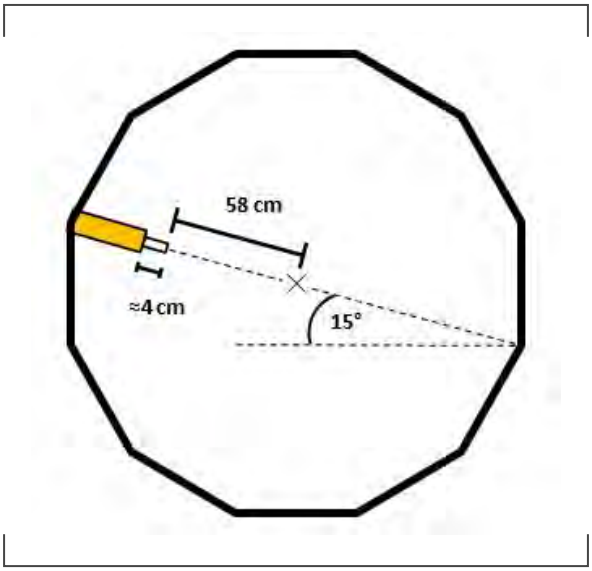

height. Initially it may be more useful to not attach the two blocks properly, so that the microphones are more accessible for calibration (this approach was taken for all measurements described in this report).

3.4.2. Theme: Low-Reflectio Rear and Front Walls

Subtask*: Assemble materials (BASOTECT foam, perforated sheet, string) for front and rear panels*

Subtask*: Sow BASOTECT onto perforated sheet with enough stitches to hold the BASOTECT in place when the perforated sheet is suspended.*

Subtask*: Adjust aluminium structure over nozzle so that channel can move further upstream. Screw a horizontal bar in place from which to suspend the front-wall elements at either side of the nozzle (with screws and sliding blocks).*

Subtask*: Screw a 180 cm metal angle to the top of the cupboard at the rear of the room. Angle has holes to attached rear wall elements (two screws each) symmetrically about the midpoint (i.e. jet axis).*

Abbildung 3.17.: **Positioning of ring microphones with respect to jet axis. Not to scale.**

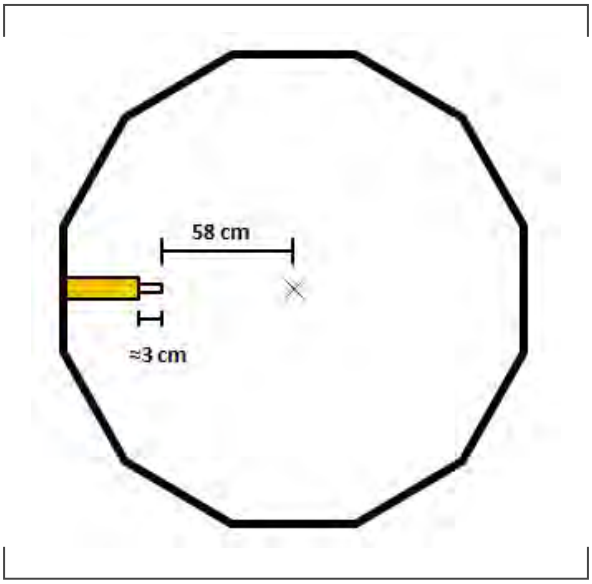

Subtask*: Suspend rear and front wall elements with long screws which fi through the perforated sheet. Use blocks of wood under the rear-wall elements for extra support, and to prevent excessive forces on the BASOTECT from the strings – which could lead to tears. Elements can be removed and re-suspended as required for access. Figure 3.19 shows the front wall on one side of the jet, the rear wall can also be seen in the background.*

3.4.3. Theme: Snow-Flake Data Acquisition System

Subtask*: Set up system according to user manual ([22]). Record all connections in a table (see appendix C).*

Subtask*: Test all connections with signal generator in place of microphones.*

Subtask*: Test with one microphone and piston-phone to ensure signal is as expected.*

Abbildung 3.18.: **Photograph of temporary stand built to represent jet axis. Taken 03/08/15.**

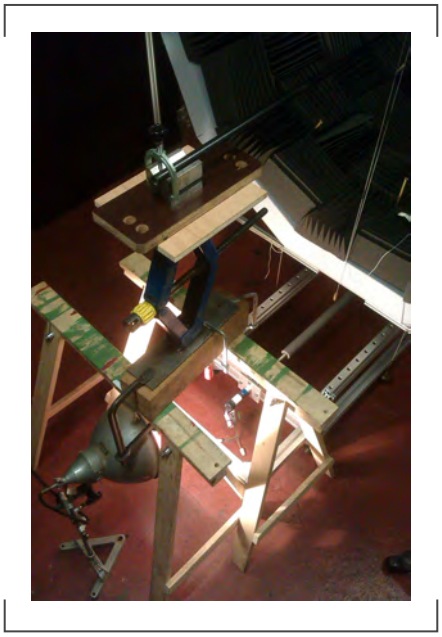

3.4.4. Theme: Linear Array

Task: Preparation of Brass Pipes

Details*: Brass pipes of length 38 cm, with hole ~6 mm diameter 8 cm from one edge.*

Subtask*: Polish outside with finishin pad (Scotch-Brite Very Fine, Red A-VFN finishin pads were used)*

Subtask*: Clean interior of pipes with pipe cleaners (German: Pfeifen Reiniger), pulled through by wire (3 pipe cleaners hooked to end of wire.*

Subtask*: Sort pipes by internal diameter (7.4 mm marked '4', 7.3 mm marked '.')*

Abbildung 3.19.: **Photograph of rig showing one low-reflectio front wall element. Taken 03/09/15.**

Task: Aluminium Holder

Details*: See figur 3.20 for schematic. [Wolfram Hage]*

Abbildung 3.20.: **Design for Linear Array Aluminium holder. [Wolfram Hage]**

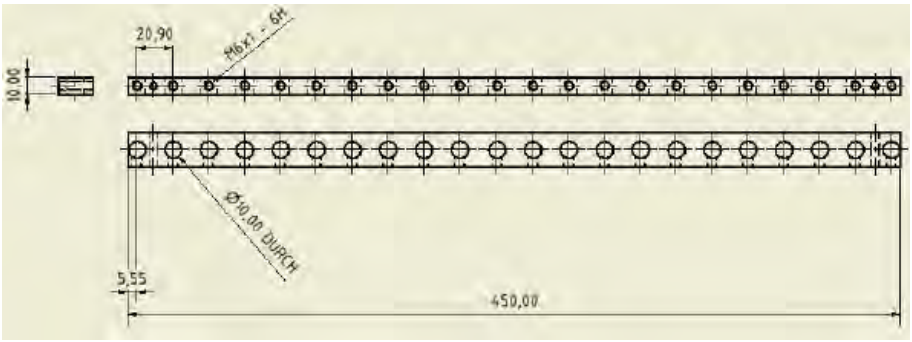

Subtask*: Create holder: holes for pipes at 20.9 mm spacing with tapered holes for plastic screws to hold pipes in place. Two additional tapered holes for screws to attach to corner element. Corner element to position. Additional tool ordered and used to slightly increase hole diameter so that pipes fi in. All steps carried out at in-house metal workshop.*

Subtask*: Screw holders in place on anechoic channel segments A-C at easily accessible height (cables and access). Ensure they are all at the same height.*

Subtask*: Twist brass pipes into position in the slots needed (see section 3.1). Pipes twisted in as far as practical: 2 cm of pipe sticking out of holder on exterior side. Once all pipes are in correct position, fi position with plastic screws.*

Task: Insulation and Connection of Microphones

Details*: Using G.R.A.S 40BP microphones with Type 26AC pre-amplifiers The pre-amplifie length is 107 mm, and to distinguish this length of pre-amplifie from the other (shorter) length available they will here be referred to as long pre-amplifiers"(http://ww .gras.dk/26ac.html)*

Subtask*: Assemble G.R.A.S microphones with long pre-amplifier (not enough available so using short pre-amplifier for the last two positions and for the ring)*

Subtask*: As some microphones were found to have deposits of oxide on the casing and the membrane, these were carefully cleaning. A fin brush and micro-fibr cloth were used to clean the membranes, which were carefully inspected by magnifying glass throughout. The protective cage was cleaned using pressurised air.*

Subtask*: Insert microphones to tubes and secure using shrink tube and tape at precise position (sticking out 4 cm from the end of brass tube). The shrink tube should be long enough to cover all of the metal of the pre-amplifie housing that is within the tube, and thus provide electrical insulation [Lech].*

Subtask*: Connect microphones to break-out-boxes, wrap up wires using Velcro straps.*

Subtask*: Run snowflake to identify channels with problems. Check connections and swap microphones to identify issues such as faulty microphones / connections.*

Subtask*: Use multimeter to check microphones are electrically insulated.*

Task: Calibration of Microphones

Subtask*: Build a stand to lie the piston-phone on so that this does not have to be held by hand. The stand consists of a plank of wood running through the channel and can be seen in the photographs in figur 3.21.*

Abbildung 3.21.: **Photographs of calibration with octopus extension. Taken on 20/08/15**

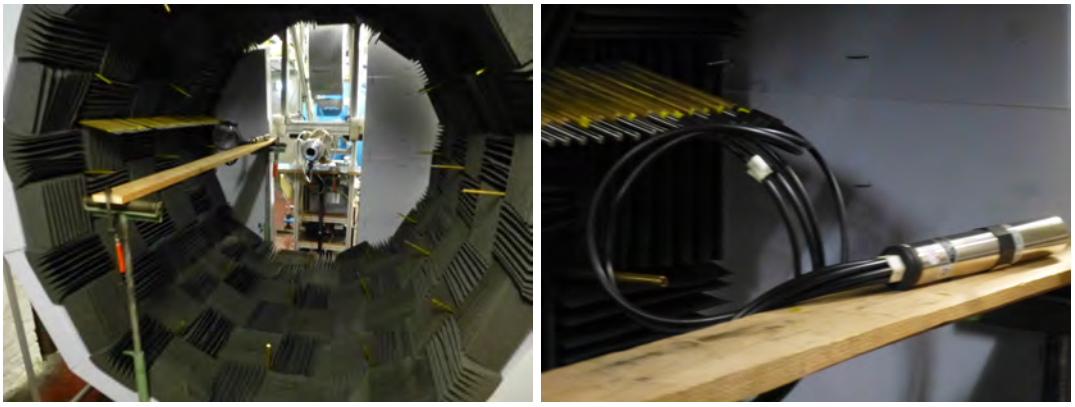

Subtask*: Connect piston-phone to octopus - connect to six microphones at a time. Ensure all six connections are filled leaving some open will result in erroneous measurements on the others*

Subtask*: Position sound-insulating front wall to block noise from snowflak computer (see section 3.4.2) (not essential).*

Subtask*: Take calibration measurements with snowflak following standard calibration protocol, using an octopus piston-phone extension and recording in a specialised log-sheet (see appendix C). The calibration sampling frequency is set to approximately 10 kHz, the calibration time to approximately 2 seconds.*

Subtask*: Analyse measurements with new Python calibration script* jextra_cal.py *(see Section 4.2).*

3.4.5. Theme: Microphone Ring

Details*: Microphones are installed into one of the rings on the anechoic channel to see what kind of results can be obtained from these. The ring chosen for this is the ring in segment B, which is at a polar angle of roughly 60 degrees.*

Subtask*: Install G.R.A.S microphones with small pre-amplifier (due to availability) into ring. Hold in position using tube and tape, as for linear array. Use ruler to determine radial position (unfortunately this has low accuracy).*

Subtask*: Take calibration measurements with snowflak following standard calibration protocol, (see above).*

4. Calibration of Microphones

4.1. Calibration Theory

4.1.1. Mathematical Basis

The key equation for the calibration of microphone-measurement-chains with piston-phones can be derived from the definitio of SPL:

$$SPL = 20\log\left(\frac{\tilde{p}}{p_{ref}}\right)$$

where $\tilde{p} = p_{rms}$ is the sound pressure. p_{ref} is a reference pressure, and SPL is the sound pressure level [5].

For calibration we consider the true pressure $p(t)$ to be the product of the raw measured value $d(t)$ and a calibration factor s, thus:

$$\tilde{p} = \tilde{d}s$$

where $\tilde{p}$ is called the sound pressure, and the tilde represents an rms value of the fluctuatio [5].

Subbing in for $\tilde{p}$ in the equation for SPL:

$$10^{SPL/20} = \frac{\tilde{d} * s}{p_{ref}}$$

Which leads to an equation for s:

$$s = \frac{p_{ref}}{\tilde{d}} 10^{SPL/20}$$

This is the standard calibration equation, where s is the calibration factor, p_{ref} is a reference pressure, $\tilde{d}$ is the raw measured signal and SPL is the known sound pressure level of the piston-phone used.

The traditional method of calibration is to use:

$$\tilde{d} = d_{rms}$$

where d_{rms} is the rms value of the time signal measured.

However, when measuring in noisy environments, as is often the case for fiel measurements, the rms value of the time signal contains a lot of noise from sources other than the piston-phone leading to an inaccurate calibration.

In order to avoid this loss of accuracy a number of alternative methods have been developed which involve a fourier transformation to the frequency domain. In the frequency domain, pressure fluctuation that correspond to the piston-phone can be singled out from background noise at other frequencies. These alternative methods are discussed in this section.

Note that technically s should be seen as a conversion factor between the raw data and pressure values rather than a true calibration factor.

4.1.2. Calibration Methods

The calibration methods discussed in this section are:

1. $\tilde{d}$ from rms value of time signal

2. $\tilde{d}$ from TOB corresponding to pistonphone frequency. (Hanning window with either PS or PSD)

3. $\tilde{d}$ from peak of power spectrum with flatto window

RMS

The standard normed method of calibration is to use the rms value of the time signal, which is calculated directly from the raw time signal measured as follows:

$$d_{rms} = \sqrt{\frac{1}{n}\sum_{i=1}^{n} d(t_i)^2}$$

TOB with Hanning PS or PSD

The PSD (power spectral density) or PS (power spectrum) (discretised into frequency narrow-bands) can be calculated using the scipy.signal.welch *function in python. The following equation gives the relation between these and $\tilde{d}$:*

$$\tilde{d}^2 = PSD * \Delta f = PS_{window} / ENBW_{window}$$

where PSD and PS are the linear power spectral density and linear power spectrum respectively of the raw time signal $d(t)$. Δf is the narrow-band bandwidth and ENBW is the Equivalent Noise Band Width, which is a correction factor based on the windowing method used. Different types of window will result in different values of PS and ENBW, but the product of these is independent of the method used. The ENBW for a Hanning window is 1.5 .

Flat top

The fla top method also uses the scipy.signal.welch *function in python. The function is used to generate a power spectrum with a flat op window. The value for the power spectrum at the maximum will exactly equal $\tilde{d}^2$.*

4.1.3. Comparison of methods for test case

The agreement between RMS, TOB and flatto methods is very good. Refer to the Wiki on microphone calibration for a quantitative comparison based on a test case generated from JEXTRA data.

N.B. the units of the original raw time series data are irrelevant to the process.

4.2. Calibration Script jextra_cal.py

jextra_cal.py *is a calibration script for the calibration of microphones using pistonphones. The methodology is loosely based on pre-existing scripts in C and python. The calibration is based on an FFT using a flatto window with the* scipy.signal.welch *python package.*

4.2.1. Overview of Methodology

1. Read command line arguments specifying the folder containing calibration data, and properties of the calibration set-up (eg. piston-phone used).

2. Read file-name in folder, then cycle through, loading and checking data.

2.1 Read the .set fil with read_adat_set *to obtain information about the data set.*

2.2 adjust_range_variables *provides some basic error control to ensure the command line input matches what is specifie in the .set file*

*3. Find which channels contain calibration signals (*find_channel *).*

3.1 Cycle through the channels in each .bin fil

3.2 Select a short snippet of the time signal.

3.3 Use signal.welch *to calculate the power spectrum of the signal, using a Hanning window.*

3.4 Correct for the FFT window with a factor of 1.5 .

3.4 Convert the power spectrum into TOBs using spec_tob_oct*.*

3.5 Select the TOB corresponding to the calibration frequency and compare this to the average to identify which channels have calibration signals.

*4. Calibrate the channels with calibration signals (*calibrate_channels*).*

4.1 Cycle through the channels containing calibration signals in each .bin fil

4.2 Use signal.welch *with a fla top window to calculate the power spectrum of the entire time signal.*

4.3 Select the maximum and then take the square root to fin d_{top}

4.4 Apply the octopus correction factor (r_{oct}*) if relevant.*

4.5 Calculate the calibration factor s *from* d_{top} *and the known piston-phone SPL*

4.2.2. Input

Path of folder containing .bin and .set calibration files
Frequency of piston-phone used.
SPL of piston-phone used.
(Optional) octopus correction factor.
First sample to consider.
Last sample to consider.
First channel of interest. (-i.e. connected to a microphone)
Last channel of interest. (-i.e. connected to a microphone)
Verbose parameter to control command line and graphical output for inspection and de-bugging.

Note that the pythonic channel numeration begins at 0, so is equal to the snowflak channel numeration - 1.

4.2.3. Output

The main output of the script is a fil containing the calibration factors for different channels. If the same channel has been calibrated multiple times, all the resulting calibration factors are listed for inspection, along with the names of the file they have been calculated from. This allows for manual inspection and comparison to the calibration log sheet. A calibration table in the correct format for use can then be created manually.

4.2.4. Results

The figure in this section show comparison between the results from calibration on two different days, both using the flatto method described above. Faulty microphones can be identifie by large differences in calibration values. In general, the match between the two calibrations, carried out two weeks apart is very good.

The calibration script jextra_cal.py *was used in both cases, in version 3a. The resulting calibration tables were manually compared to the log sheet, and a condensed calibration table with one factor per channel was created in the suitable format. These calibration tables are saved in the following files*

JEXTRA_calibration_table_200815.txt
JEXTRA_calibration_table_030915.txt

Figure 4.1 shows that the calibration factor for channel 45 as calculated on 03/09 is several orders of magnitude higher than expected. This agrees with the comment 'channel 46 very low' recorded on the calibration log sheets, and suggests a faulty microphone.

Figure 4.2 shows the same plot as Figure 4.1, but with a reduced scale. It is clear that the variation in the calibration factors for channels across the two days is, with the exception of channels 14 and 15, much lower than the variation in calibration factor between different channels. The uncharacteristically low values of calibration factor calculated on 20/08 for channels 14 and 15 could be explained by the fact that for this measurement only two of six arms of the octopus-piston-phone-extension were connected, rather than the full six that were used for every other measurement.

Abbildung 4.1.: **Comparison of calibration factors for calibration on 20/08 (blue) and 03/09 (red).**

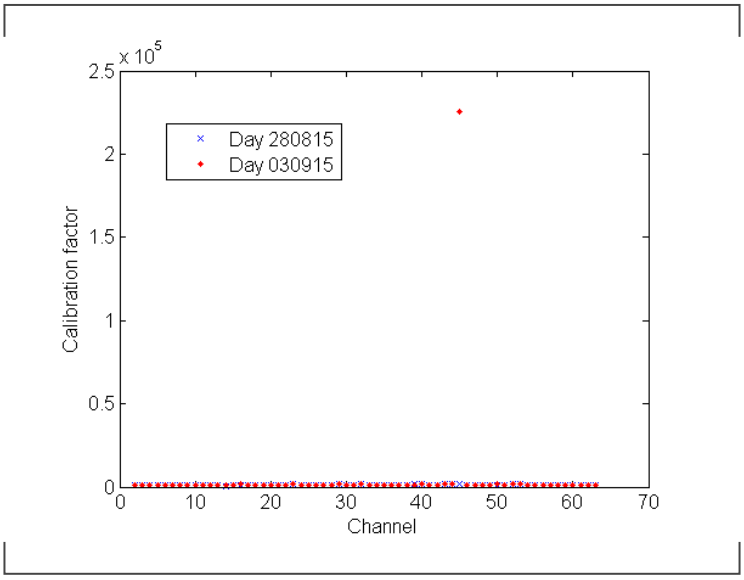

In Figure 4.3 the percentage discrepancies between calibration factors are shown. The 3 cases where errors are suspected (discussed above) are not included in this plot. The percentage variation in calibration factor is below 0.04 % for all other channels.

Finally, Figure 4.4 shows the logarithmic difference between the calibration factors, which is most relevant as it is the SPL of the sound signal that will be inspected. Not taking into account the three erroneous cases, the value is below 0.32 for all channels.

Abbildung 4.2.: **Comparison of calibration factors for calibration of 28/08 (blue) and 03/09 (red). Channel 45 off scale.**

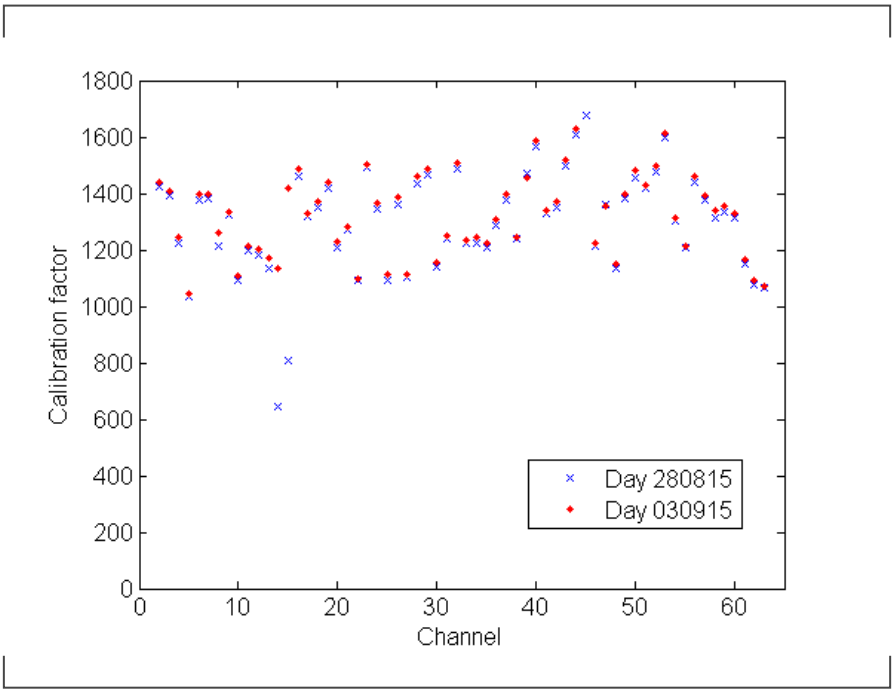

Abbildung 4.3.: **Percentage discrepancy in calibration factors between measurements from 20/08 and 03/09**

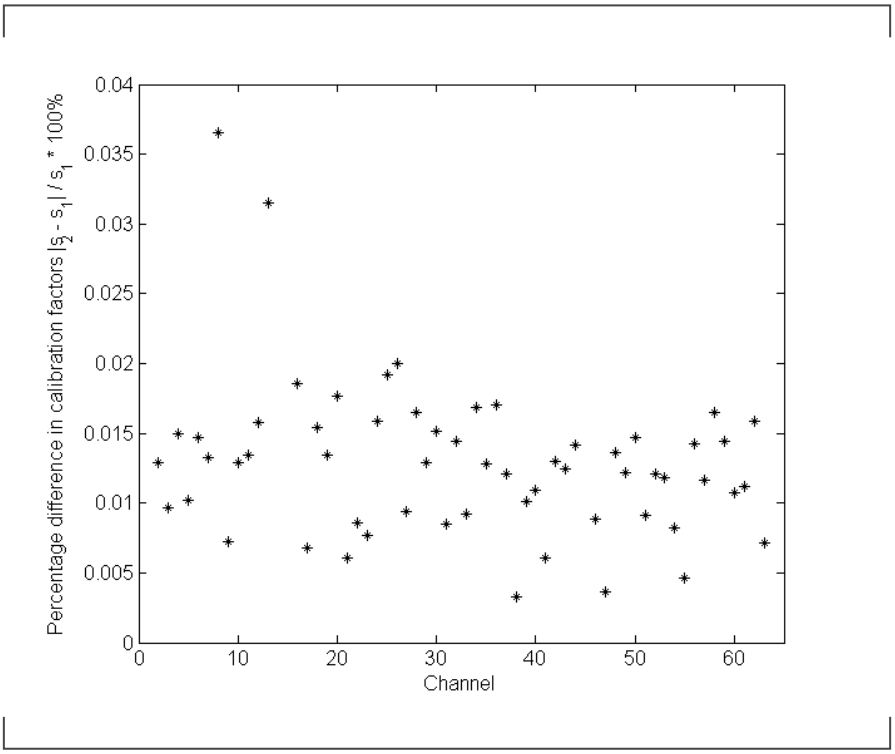

Abbildung 4.4.: **Logarithmic difference in calibration factors between measurements from 20/08 and 03/09**

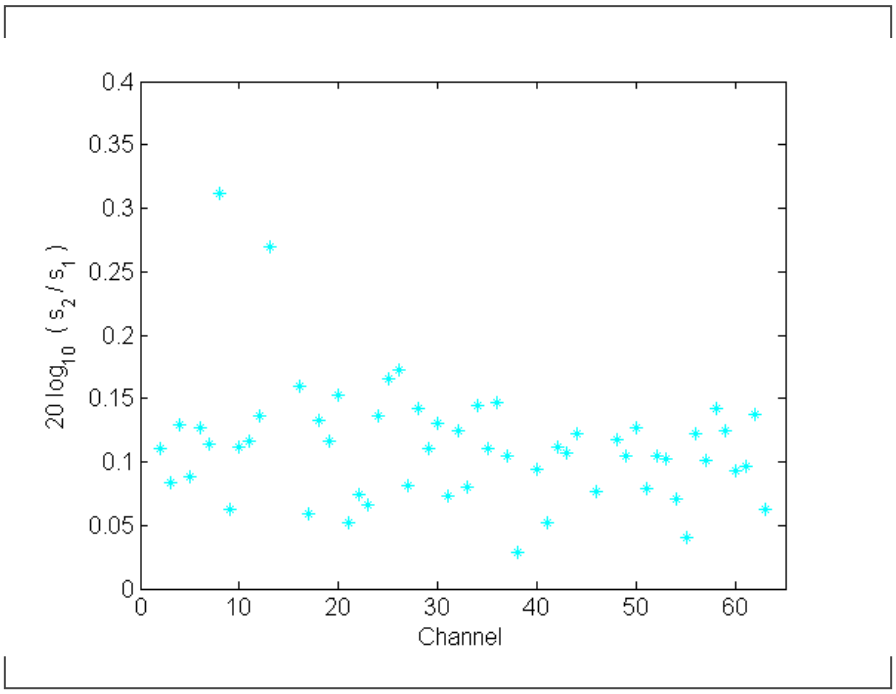

5. Single Source Reflectio Experiments

In order to verify the anechoic properties of the experimental rig, a series of tests using single sound sources were conducted to investigate what reflection can be observed. An ideal 'single sound source' is, in this context, define as a sound source which generates an impulsive pressure signal in the time domain radiating from a single point in the space domain. In practical terms, this means a short, loud signal originating from a small area. In order to achieve this, two methods were attempted. The popping of a rubber membrane using air pressure, and firin a blank gun. Photographs of the experimental setup can be seen in section 5.1. The results of these 'single sound source' experiments are presented and analysed in this section.

5.1. Experimental Set-up

Experiments measuring the microphone array's response to an impulsive sound source were carried out in order to identify reflection and other issues with the array. In order to achieve an approximately impulsive signal, two methods were used. The firs involved popping a thin 'rubber' membrane, which was carried out at the nozzle exit and at fiv nozzle diameters downstream of the nozzle exit. The measurements at fiv nozzle diameters were carried out because it is possible that, for a sound source at the nozzle exit, the nozzle itself will scatter the sound signal and thus lead to unrepresentative results. A distance of fiv nozzle diameters was chosen, as the literature suggests that at this location there is a peak in sound generation in the jet [5].

The second method used a blank gun. The blank gun needs to be held by hand, so its positioning is less accurate. The position aimed for was approximately two nozzle diameters downstream of the nozzle exit in order to avoid scattering effects due to the nozzle.

5.1.1. Pop

A thin 'rubber' membrane (cut from blue rubber gloves) was stretched over a metal bicycle-pump-valve-adapter and firml attached by string. By pumping air into the pipe using a bike pump, it is possible to burst the sheet (similar to popping a balloon) and thus achieve a 'pop' sound. This 'pop' is a reasonably impulsive sound signal. Figure 5.1 shows the construction.

Abbildung 5.1.: **Photograph of the thin 'rubber' sheet (blue) stretched over a metal pipe segment which connects to a bicycle pump. The 'rubber' sheet is firml tied in place with (black) string. Taken 20/08/15.**

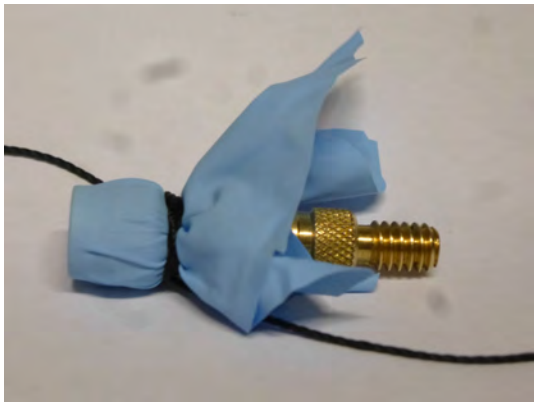

The bike pump used was clamped to the underside of a wooden board situated just below and upstream of the nozzle (figur 5.2). In order to pop the 'rubber' fil the operator pushed the pump handle upwards towards the wooden board. The set up was later improved by tying a piece of foam to the pump, which softened the sound of the pump handle hitting the pump when it was pushed right to the top. This modificatio is not shown in the photo.

Pop at Nozzle exit

The position of the popping contraption can be seen in figur 5.3

Pop at 5D

The position of the popping contraption can be seen in figur 5.4. Note that the position is slightly off-centre.

Abbildung 5.2.: **Photograph of the bicycle pump clamped to underside of wooden board for 'pop' single sound source tests. Taken 20/08/15.**

5.1.2. Blank Gun

In order to generate a loader sound, a blank gun was fire within the anechoic channel. The gun was held by hand, with the sound source at roughly 10 cm from the nozzle exit, as can be seen in figur 5.5.

5.2. Results

5.2.1. Time Signals

Figures 5.6 to 5.8 show the response of the linear array microphone at a polar angle of 52.3°. The y-axis shows pressure while the x-axis shows time multiplied by the speed of sound, so give a measure of how far the sound has travelled. The plots only show data for a few meters past the initial impulse, as after this the signal decays away, and no further artefacts of interest can be identified The pressure initially decreases, before increasing, which could be due to the phase of the microphones.

The pop at the nozzle seems to give the cleanest impulse, while the signal from the blank gun, which it was assumed would be superior is less clean.

Abbildung 5.3.: **Photograph of rubber-membrane construction at the nozzle exit. Taken 20/08/15.**

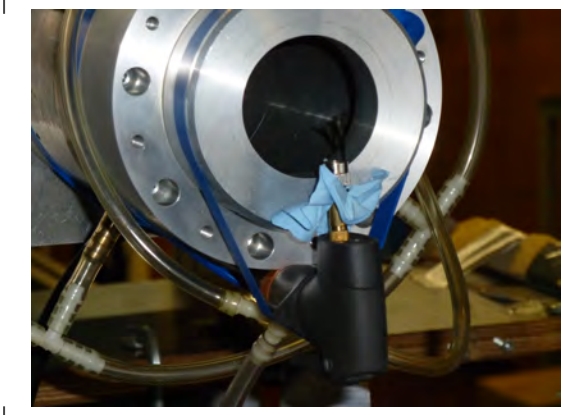

Abbildung 5.4.: **Photograph of rubber-membrane construction at fiv nozzle diameters from the nozzle exit. Taken 20/08/15.**

These time signals, and those for all other microphones were analysed to produce reflecti on contour maps. A Hilbert transformation is carried out to fin the envelop of the signal, the pressure value is then converted to an SPL. Contours of SPL on a grid of distance travelled by sound against distance of microphone from nozzle can then be plotted. These contour maps can be seen in section 5.2.2.

Further analysis suggested for future work would be to calculate signal to noise ratios, and look at the data in the frequency domain.

Abbildung 5.5.: **Photograph of Blank Gun held in position. Taken 20/08/15.**

5.2.2. Reflectio Contour Maps

In order to observe the pattern of reflection on the entire microphone array contour maps have been generated. Contours of Sound Pressure Level are shown on an axis of time versus microphone position. The time axis is converted to show the distance travelled by sound (with an arbitrary zero) by multiplying the time intervals with the speed of sound.

As sound pressure is a fluctuatin value, a Hilbert transformation was carried out to fin the envelope. The absolute value of the Hilbert transform is then converted to a sound pressure level. The python script jex_quick_look.py *contains all these steps, and is available on the JEXTRA hard drive.*

Results

Figure 5.9 shows the microphone response to a gun shot. Firstly it should be noted that after the initial signal, all further pressure fluctuation are more than 20 dB under the initial impulse in magnitude. The suggests that the anechoic set-up is very effective at reducing reflections A comparison to a test case with no sound insulation would be useful to provide a quantitative assessment. The sounds close to the initial impulse are likely to be due to scattering at the nozzle, while the faintly visible sounds at that have travelled a further distance are most likely to be caused by reflection from the rear wall. It will be shown later that there shape fit very well to the expected shape for reflection from walls perpendicular to an array and that the distance travelled by the sound for the closer of the two corresponds very well to a reflectio from the back wall of the room.

Abbildung 5.6.: **Time signals of microphone response to pop at nozzle. Microphone at polar angle of 52.3°.**

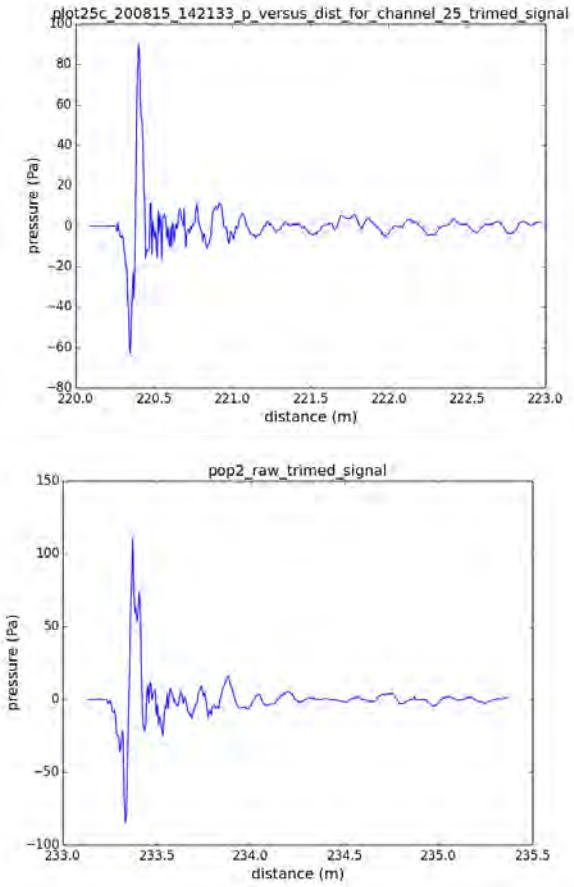

This suggests line at around 10 m sound travelled corresponds to a second reflection in other words that sound wave reflect firs off the back wall then off the nozzle or other constructions at the front before reaching the microphone. Both of these 'long distance' reflection are only very low in amplitude, and thus their effect on jet noise measurements will be minimal.

Figure 5.10 shows the same data but focused in on the region around the impulse, and with a lower SPL dynamic, of just 30 dB.

Results for the pop experiments and the other blank gun experiments look very similar, an have thus been omitted here.

Comparison to Room Geometry

A simple MATLAB simulation of reflection from different artefacts in the room was carried out. The simulation takes into account the law of reflection that the angle of reflection is equal to the angle of incidence, and uses this to calculate distances that sound waves would travel between a source at the nozzle and the microphone.

Figure 5.11 shows the reflection contour map for the fourth blank gun measurement, with reflection simulations superimposed. The distance between the nozzle and the microphone (plotted in black) is used to align the reflection contour map with its arbitrary zero in the y axis, and the simulation results. The magenta line represents a reflection from the opposite wall of the anechoic channel. This falls in the region where the reflection contour map shows some evidence of reflections but at a magnitude much lower than the original signal. The red line represents a reflection from the low-reflection rear wall. This matches very well in shape and position to a line that can be observed faintly on the reflection contour map, suggesting that there is indeed a reflection from the rear wall. The SPL of this reflection is around 30 dB lower than the original impulse, so this is not an issue.

5.3. Conclusions of Validity of Anechoic Channel

There are no major issues with reflection for the experimental set-up. A quantitative assessment of how effective the 'anechoic' channel is would require a similar set of measurements to be carried out in the room, without the 'anechoic' channel in place. This is recommended for future work on the project.

N.B. A further single source experiment has been carried out with a reflective board placed inside the anechoic channel. The measurements from this experiment are available, but the analysis has not been carried out at time of writing.

Abbildung 5.7.: **Time signals of microphone response to pop at fiv nozzle diameters from the nozzle exit. Microphone at polar angle of 52.3°.**

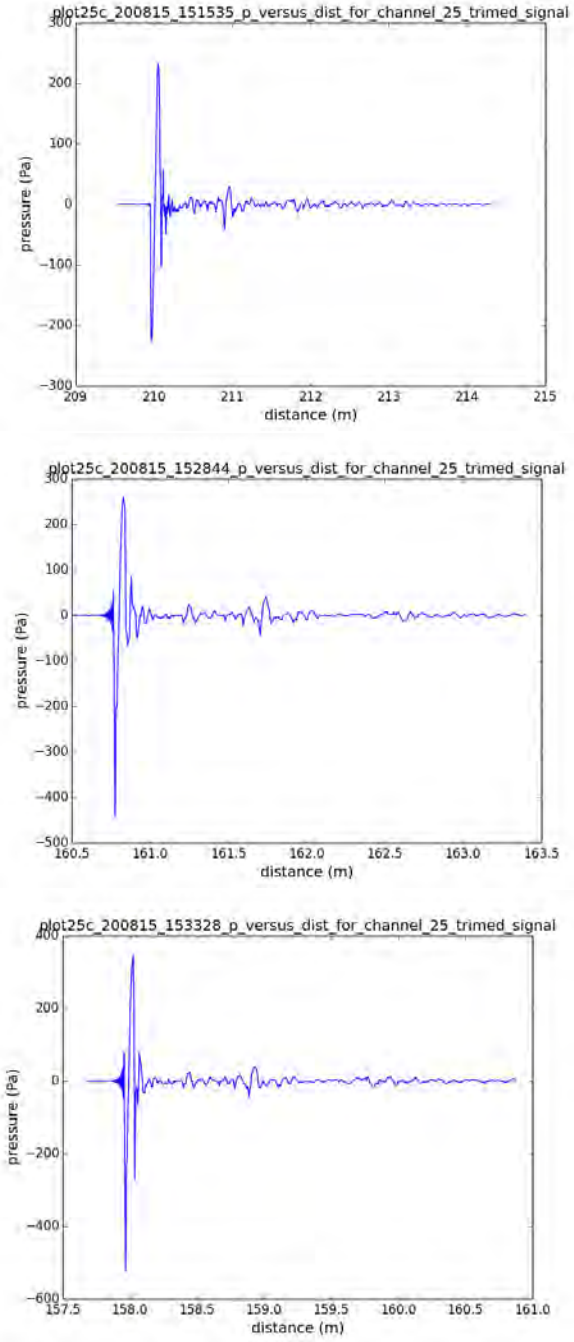

Abbildung 5.8.: **Time signals of microphone response to blank gun shot at two nozzle diameters from the nozzle exit. Microphone at polar angle of 52.3°.**

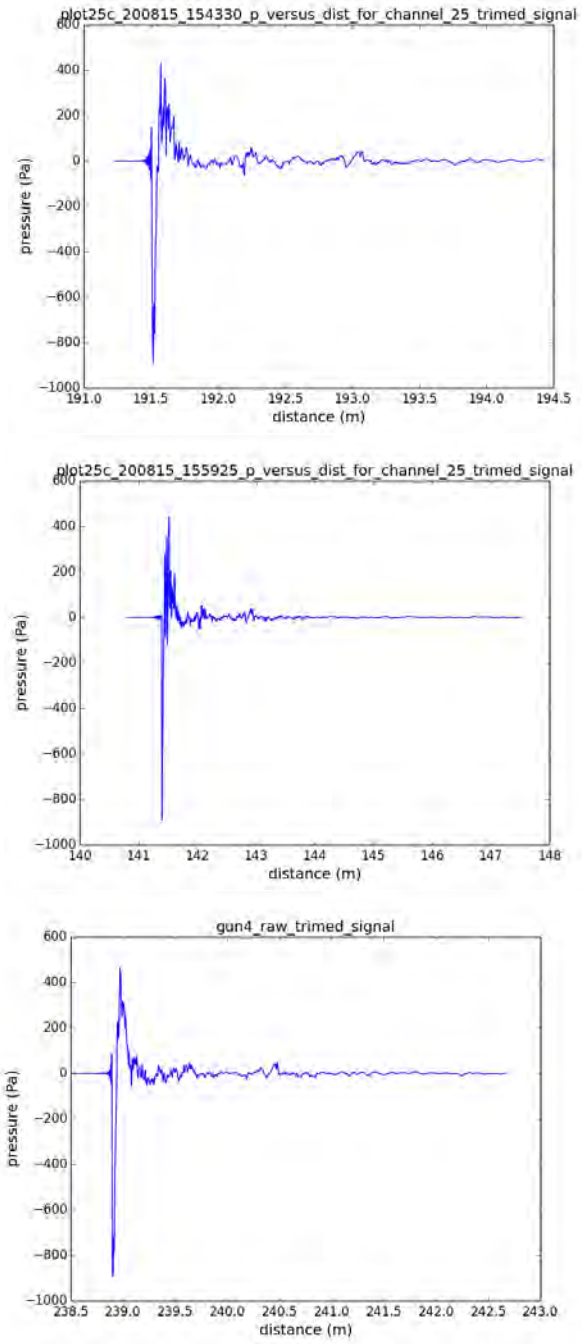

Abbildung 5.9.: **Contours of SPL an axis of distance travelled by sound versus microphone position. File: Showing 20 m travelled by sound. SPLs for each channel shifted to set the maximum to zero. Thus direct comparison of SPL between different microphones is not possible.Dynamic of 40 dB**

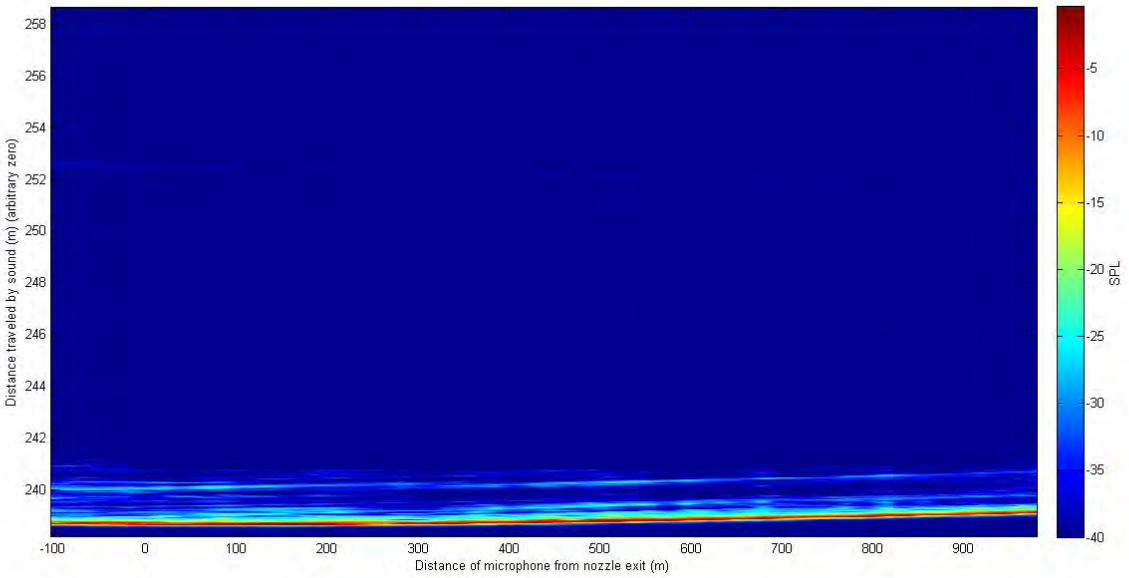

Abbildung 5.10.: **Contours of SPL an axis of distance travelled by sound versus microphone position. File: Showing 4 m travelled by sound. SPLs for each channel shifted to set the maximum to zero. Thus direct comparison of SPL between different microphones is not possible.Dynamic of 30 dB**

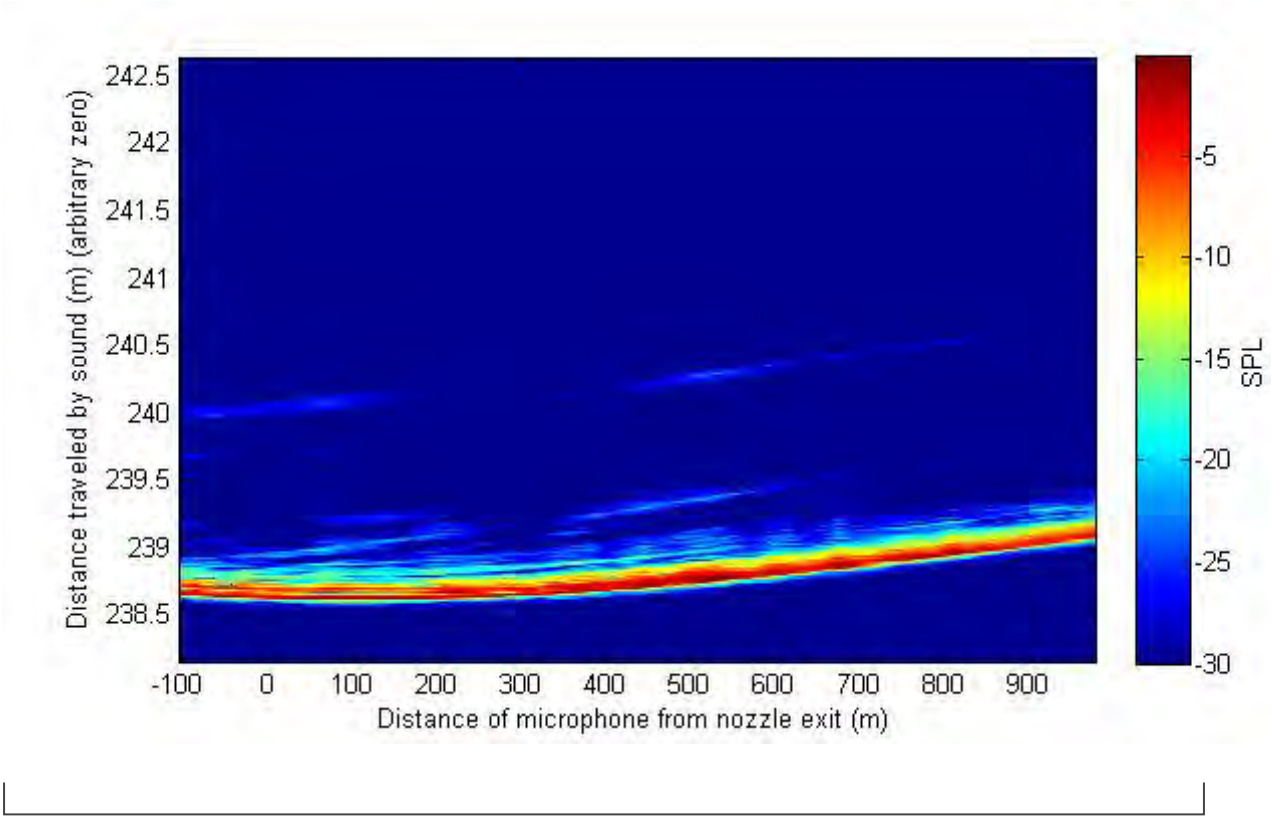

Abbildung 5.11.: **Simulated reflection**

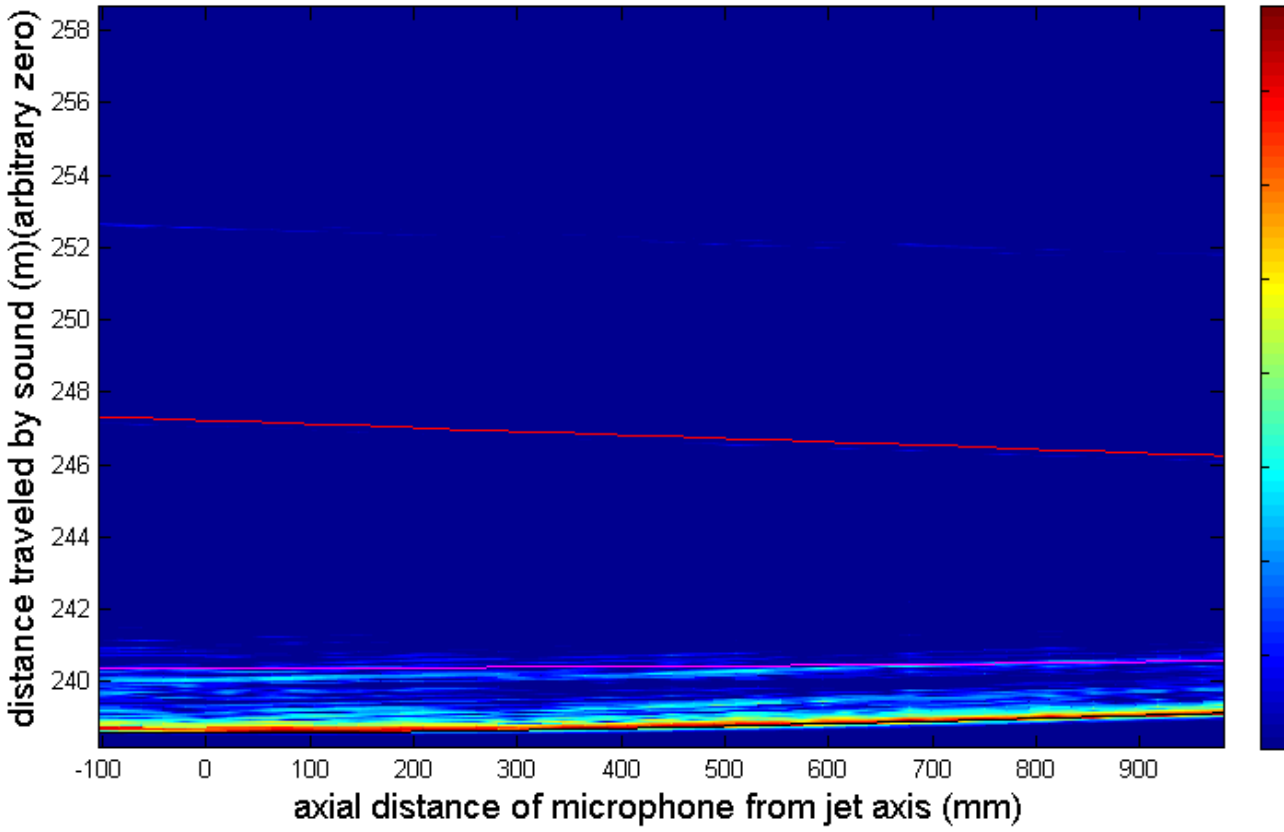

6. Jet Noise Measurements

6.1. Basic theory

The potential core of the jet extends 4 - 5 nozzle diameters downstream of the nozzle exit. At the boundary between the jet flo with the outer ambient flo a shear layer forms. The instability of this shear layer generates turbulent structures. These turbulent structures start off small, close to the nozzle exit, and grow into larger turbulent structures towards the end of the potential core, before these fall apart again into small structures. [5] The key regions are shown in the schematic in figur 6.1.

Abbildung 6.1.: **Schematic of jet showing shear region and potential core.**

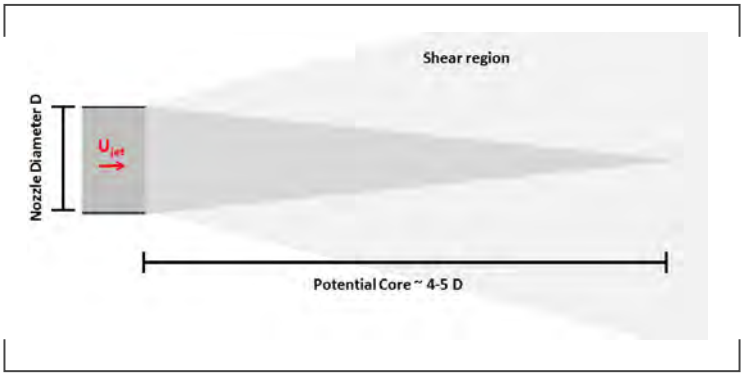

The fine-scal structures (FSS) near the nozzle exit are associated with high frequency components. The large-scale structures (LSS) are associated with lower frequency sound. The high frequency FSS sound is radiated primarily to high observer angles, while the lower frequency LSS sound can be measured at smaller observer angles. [11] See figur 6.2.

The different scales of turbulent structures are associated by Karabasov with two distinct physical mechanisms of jet noise. The physical mechanism for FSS is the pressure exerted by fine-scal turbulence in the shear layer, which is equivalent to classical lighthill acoustic analogy. The physical mechanism suggested for LSS is the growth and decay of linear instability waves [11].

Abbildung 6.2.: **Directivity of sound from different regions of the jet.**

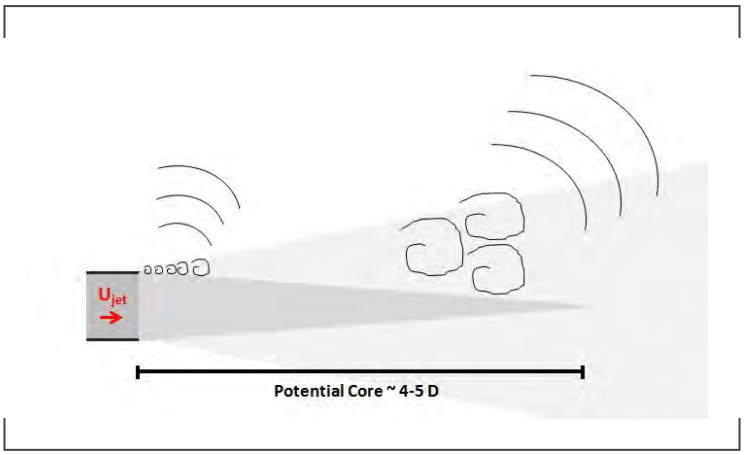

A more extensive overview of jet noise theory can be found in the Aircraft Noise Course Lecture Script by Ulf Michel and Henri Siller [5].

6.2. Experimental Setup

The acoustic measurement set-up is discussed in detail in chapter 3. For details about the jet set-up contact Robert Meyer, Alessandro Bassetti or Karsten Liesner.

The Mach number at nozzle exit is determined from 1D compressible flo theory.

$$M = \sqrt{\frac{2((p_0/p)^{\gamma-1/\gamma} - 1)}{\gamma - 1}}$$

where p_0 *is the stagnation pressure,* p *is the static pressure and* $\gamma = 1.4$.

A program exists to regulate he rotational speed of the compressor to achieve the desired Mach number. The Stagnation pressure at exit is initially assumed to be equal to the pressure in the chamber, neglecting the change in stagnation pressure through the pipe. For more details contact Karsten Liesner.

6.3. Comparison Data

Comparison of Jet Noise measurements from the JExTRA linear array with results from 'The Generation and Radiation of Supersonic Jet Noise. Volume III, Turbulent Mixing Noise Data' *by Lockheed [9]. which contains tables for jet noise experiments with a 2 inch nozzle published in 1976.*

For details on the experimental set-up and data handling refer to the book [9]. It should be noted that an atmospheric absorption correction has been applied ot the data. The SPL results are taken directly from the tables, with no additional data handling or corrections applied.

The test cases used for comparison purposes are cases 20, 21, 22, 23. These cover a range of Mach numbers from 0.4 to 0.7 .

Figure 6.3 shows a contour map of Sound Pressure Level (SPL), on a Strouhal Number versus Microphone polar angle plane. Features typical of jet noise can be observed, such as an increase in Strouhal Number for the peak SPL as the polar angle of the microphone increases. The magnitude of peak SPL at low angles is also greater than that at higher angels, another common feature in jet noise. For the 90° measurement the peak SPL occurs at a Strouhal number of 1.8, whereas at 30°, the peak is closer to St = 0.5 .

6.4. Mathematical Considerations

6.4.1. Atmospheric absorption correction

Atmospheric absorption of sound prevents accurate comparison at microphones at different distances, even when the R^2 dependency of sound power on distance has been considered. Moreover, the absorption of sound is frequency dependent, with higher frequencies being absorbed more than lower frequencies. Thus in order to look at the frequency characteristics of a jet it is important to apply an atmospheric absorption correction otherwise the high frequency content will be under-estimated.

The general equation for atmospheric sound absorption is:

Abbildung 6.3.: **Contour Map of SPL variation for Strouhal number versus angles from downstream jet axis, for Lockheed data[9], M = 0.5. (TP 21).**

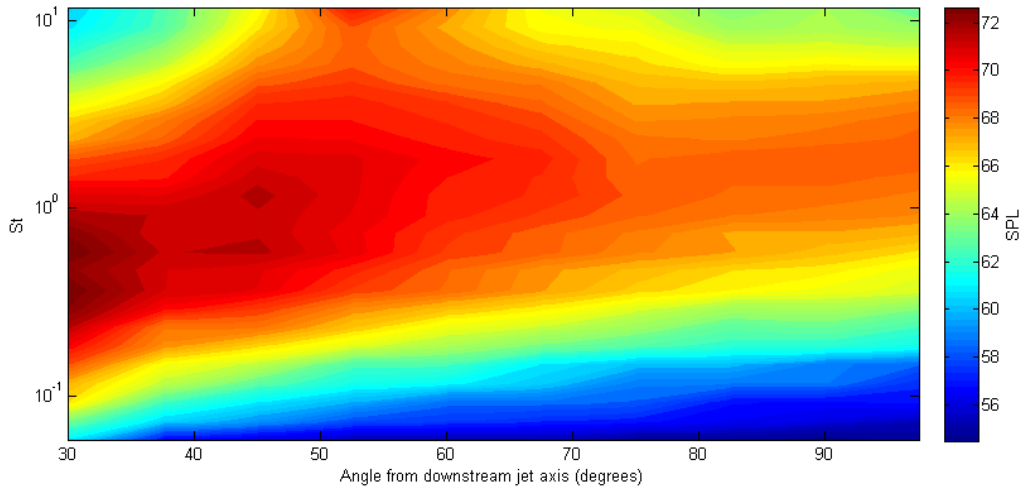

$$SPL_2 = SPL_1 - r\ 10\log_{10}(a)$$

where $\alpha(f) = 10\log_{10}(a)$ *is a frequency dependent damping coefficien usually referred to as the 'absorption coefficient' and SPL is the sound pressure level.*

The equation for $\alpha(f)$ *is quite long, and can be found as equation 1.80 in the Aircraft Noise Course lecture script by Ulf Michel and Henri Siller [5].*

Note that the atmospheric absorption correction is not a distance correction, and that it should be implemented before the distance correction. Once the atmospheric absorption correction has been applied, a distance correction can be applied to allow comparison between the JEXTRA and Lockheed data [9] (see section 6.4.2).

Applying an atmospheric correction can lead to an over-correction at high frequencies, leading to a non-physical rise in SPL at the highest frequencies. It is difficul to quantify this effect.

6.4.2. Distance correction

In order to compare the two datasets it is necessary to non-dimensionalise the frequency, by calculating the Strouhal number:

$$St = \frac{f_s D_j}{U_j}$$

The Lockheed data [9] was measured at a constant distance from the nozzle exit for all angles, whereas the JExTRA data comes from a linear array, and thus the distance increases as the angle to the downstream jet axis moves away from 90°.

In order to enable a direct comparison between the data sets it will be necessary to apply a correction to the JExTRA data based on the decay of the sound over space. In order to do this a few simplifying assumptions will be made:

1. The absorption of sound by the air has already been taken into account.

2. For a given angle and frequency sound pressure is only a function of distance (r) from the sound source.

3. The sound source is at the nozzle. (This is not technically exclusively the case, but this assumption significantl simplifie the comparison to the Lockheed data [9], as any other sound source location would mean both data sets need adjusting).

With these assumptions we can derive a relationship for the variation of SPL with r, which can be used to apply a 'correction' to the JExTRA data and allow for a more direct comparison.

Energy flu through a sphere around the source is constant.

From assumption 2, we can then say that energy flu through an infinitesimall small

area of the sphere along a line propagating radially outwards from the sound source is constant.

i.e.

$$A * 4\pi r^2 I = K = const$$

where I is the intensity, r is the radial distance and a is an infinitesimall small constant definin the proportion of the surface area through which we are considering an energy flu of magnitude K.

Simplifying and rearranging:

$$I = B / R^2$$

where $B = K / (A * 4\pi) = const$

The intensity I is given by:

$$I = \tilde{p}^2 / \rho c$$

where ρ is the mean value of density and c is the speed of sound [5].

Combining these two equations we get:

$$\tilde{p}^2 = \rho c B / r^2 = D / r^2$$

Converting to logarithmic values:

$$SPL = 10 \log(\frac{\tilde{p}^2}{p_{ref}}) = 10 \log(\frac{E}{r^2})$$

where SPL is the sound pressure level.

$$SPL = F - 10\log r^2$$

$$SPL = F - 20\log r$$

Then, as we know SPL and r for the measurement at each microphone position, we can determine a value of F for each polar angle. Once a value of F has been obtained from $F = SPL + 20\log r$*, an estimation of the SPL that would be measured at any distance* r *can be made, so it is possible to calculate an estimation of the SPL at the same distance* $r = R_{yb}$ *for each angle, thus allowing better comparison to the Lockheed data [9]. The fina equation for the correction to apply is:*

$$SPL_{\text{estimation at distance } R_{yb}} = SPL_{\text{variable distance } (r)} + 20\log(r/R_{yb})$$

6.5. Results

6.5.1. Data Correction (M = 0.5 case)

The effect of applying the data corrections described in section 6.4 are shown in this section. Figure 6.4 shows the uncorrected data for microphones at three different angles plotted on a Sound Pressure Level versus frequency axis. Figure 6.5 shows the same data after an atmospheric absorption correction has been applied. Figure 6.6 shows the data corrected for both atmospheric absorption and distance. A constant microphone distance of 3.9 m has been chosen to allow direct comparison to the Lockheed data.

By comparing figure 6.4 and 6.5 it is clear that the absorption correction does not have a major effect on the results. This is as would be expected considering that the distances between the jet and microphones are small, so very little sound absorption will have taken place. The only noticeable difference is at high frequencies. High frequencies are affected most by sound absorption, so the correction increases the SPL at these frequencies most. In the region where this increase in SPL is observable, the data already deviates from the expected jet-noise pattern, and thus it is questionable whether the results here are valid. The ring measurements show that for the M=0.5 case at above approximately 10 kHz (or St = 3), the measurements at different positions on the ring start to deviate from each other. This departure from axisymmetric behaviour casts further doubts on the validity of the data at high frequencies.

Abbildung 6.4.: **Uncorrected data for JEXTRA (02/09). M = 0.5 case.**

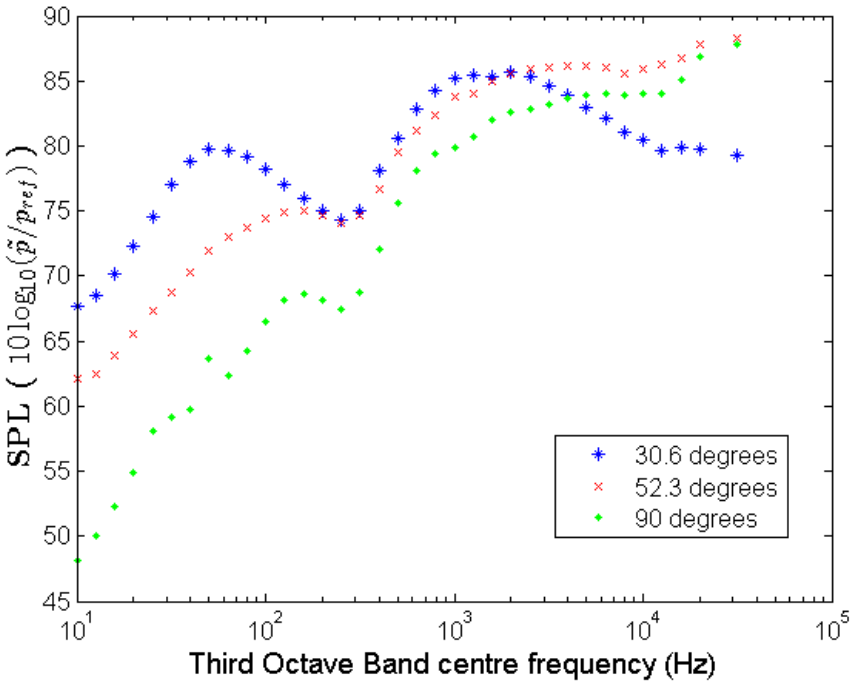

Comparing figure 6.5 and 6.6 shows that the distance correction does not change the overall patterns observed. Instead the distance correction brings the results closer to the Lockheed data in terms of the magnitude of the SPLs. Further, the difference between the positions is increased. Whereas the SPLs at different microphone positions were quite similar for the raw data, the distance corrected data very clearly shows a trend of SPL increasing as the observer angle drops, which matches the Lockheed data (see section 6.3).

Note that for all figure in this report, the frequency and Strouhal Number axes are plotted in third octave bands rather than narrow-bands.

6.5.2. SPL Contour Maps (M = 0.5 case)

Figure 6.3 in section 6.3 shows a contour map of the Lockheed data for the M = 0.5 test case, showing the variation of SPL on the Strouhal Number-Angle plane. Figure 6.7 shows the same graph for the JEXTRA data, with the atmospheric absorption and distance corrections described in section 3.1 applied. The two figure look significantl different. It must be noted that the Strouhal Number axis for the JEXTRA data covers a larger

Abbildung 6.5.: **Uncorrected data for JEXTRA (02/09). M = 0.5 case.**

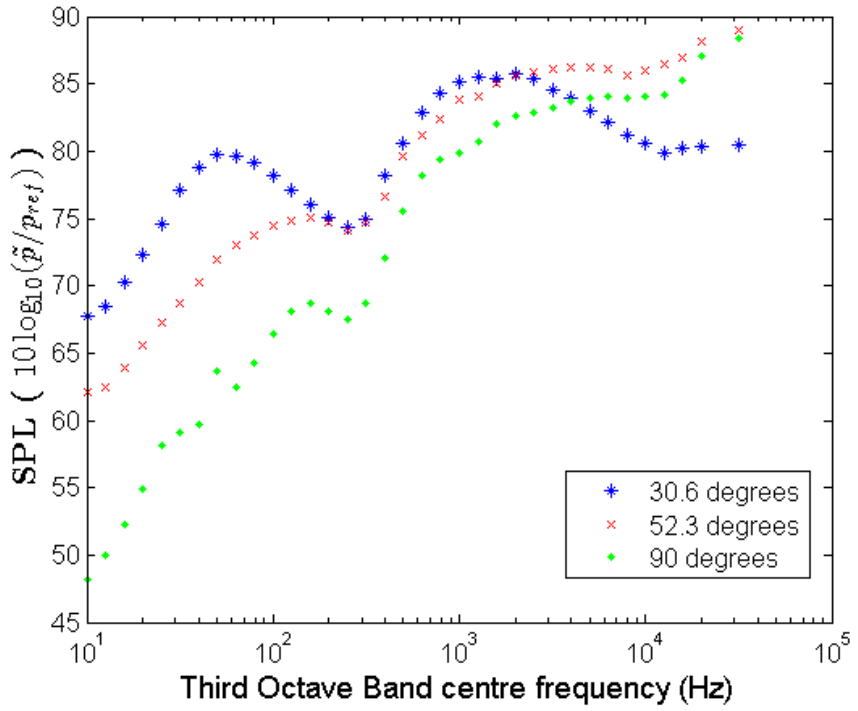

range, extending to significantl lower Strouhal numbers than the Lockheed data, while the Lockheed data extends to slightly higher Strouhal numbers. The Lockheed data also extends to lower microphone angles.

To enable a more direct visual comparison, the same data has been plotted on axis that have been reduced to cover only overlapping test points. These contour maps can be seen in figur 6.8. The general trend matches reasonably well, especially at lower angles. At higher polar angles the JEXTRA data does not reach a peak at the Strouhal numbers expected, instead the SPL continues to increase at higher frequencies, which questions the validity of these results.

The low frequency behaviour of the JEXTRA data is more clearly visualised in the single-colour plot in figur 6.9, where the SPL dynamic is limited to 30 dB, and the data is shifted so that the maximum is at 0 dB.

From Figure 6.9 it can be seen that, particularly at low angles, there is an additional low frequency peak. The magnitude of this peak is lower than the higher frequency peak, especially at higher angles. The low frequency peak varies in both magnitude and frequency for different microphone positions. It is a rounded peak which suggests that

Abbildung 6.6.: **Corrected data for JEXTRA (02/09). M = 0.5 case.**

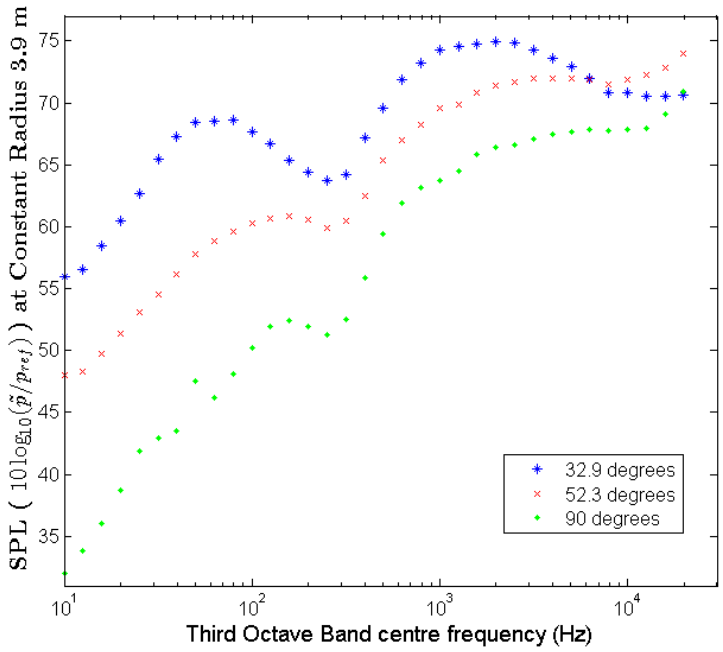

it is related to the jet. Tonal external noise sources would be expected to give a sharper peak. Mach Number exponent analysis in section 6.5.6 further supports the suggestion that the low frequency peak is linked to the flo rather than external noise.

6.5.3. SPL-St Graphs for Different Angles (M = 0.5 case)

Graphs of Sound Pressure level against Strouhal Number are shown in this section for angles at 30°, 52° and 90°.

The Aircraft Noise Course Lecture Script by Ulf Michel and Henri Siller [5] suggests that a peak in SPL at a Strouhal Number of 1.0 for unheated or 0.7 for heated jets is to be expected. The broadband nature of the peak, and the dependency of the jet on a range of external factors mean that the peak position will vary between different experimental set-ups. In general however a peak in the range St = 0.1 - 2.0 is to be expected.

Figure 6.10 gives a comparison between microphones at observer angles of roughly 30° , 52° and 90°.

Abbildung 6.7.: **Contour Map of SPL variation for Strouhal number versus angles from downstream jet axis, for JExTRA data, M = 0.5.**

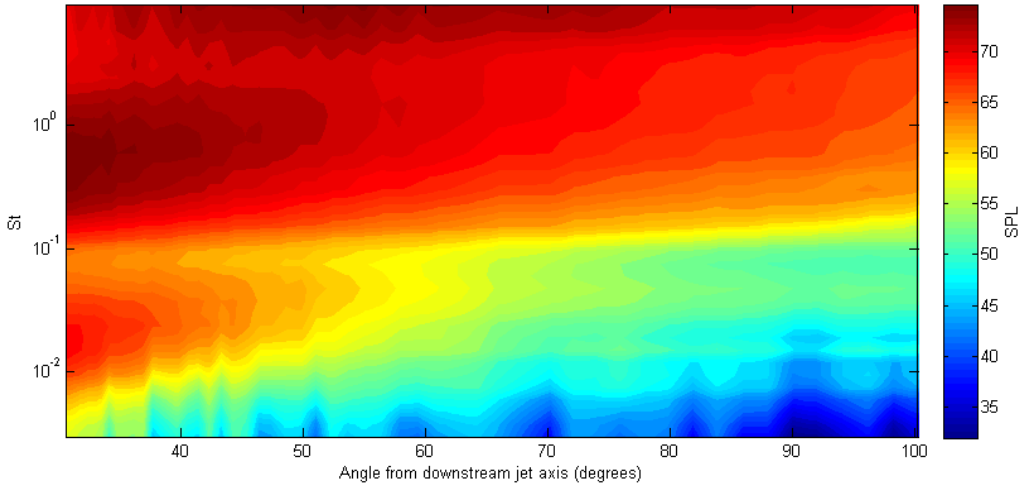

Figures 6.11 to 6.13 show the JEXTRA and Lockheed results plotted on the same graph for comparison.

The pattern agrees well in the range of Strouhal Numbers from 0.1 to 3.0. The peak in SPL occurs at roughly the same Strouhal number for all three angles presented. For the 52° and 90° cases the Sound Pressure Level is also very similar. For the 30° microphone the difference in SPL at the peak is roughly 3dB. Taking into account the fact that no near-fil correction has been applied (see section 6.5.7) to the JEXTRA data, the agreement with the comparison data is good.

6.5.4. Variation with M

Figure 6.14 shows the variation of the SPL-freq-angle characteristic with Mach number. The pattern observed is fairly consistent over different Mach numbers.

Figure 6.15 shows the data from the 90° microphone at different Mach numbers. The magnitude of SPL over the entire frequency range increases with Mach number as would be expected [5]. The Strouhal Number of the peak seems to be fairly independent of Mach number, suggesting Strouhal scaling.

Abbildung 6.8.: **Contour Map of SPL variation for Strouhal number versus angles from downstream jet axis. M = 0.5 case. Lockheed data [9] (left) and JEXTRA data (02/09) (right)**

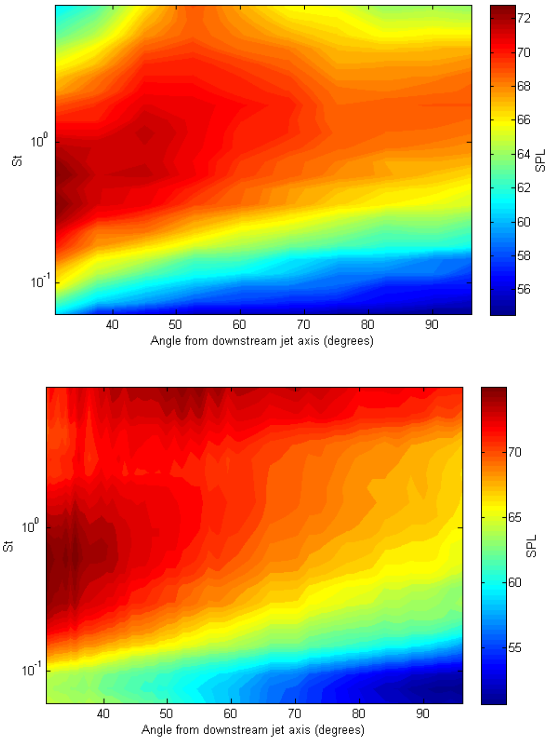

6.5.5. Experiments with Flow Conditioning in Pipe

Experimental Setup

In order to investigate whether the low frequency peak could be due to resonances in the pipe, a resistance element was built into the pipe in order to disrupt the flo and see whether differences can be observed in the sound signals.

Figure 6.16 shows the conical element and cylindrical rectifie inserted into the pipe. Figure 6.17 shows the conical resistance element inserted into the pipe. In order to accurately determine the Mach number of the flo at the nozzle, the calculation is altered to include the pressure difference across the pipe. For simplicity it is assumed that, throughout the constant area pipe the change in air density is negligible and thus, by continuity, the velocity is constant. This means that the drop in stagnation pressure across the pipe is equal to the drop in static pressure across the pipe. This assumption neglects the change

Abbildung 6.9.: **Contour Map of SPL variation for Strouhal number versus angles from downstream jet axis. Data shifted so that maximum is at 0 dB. Dynamic range of 30 dB. M = 0.5 case. JEXTRA data (02/09)**

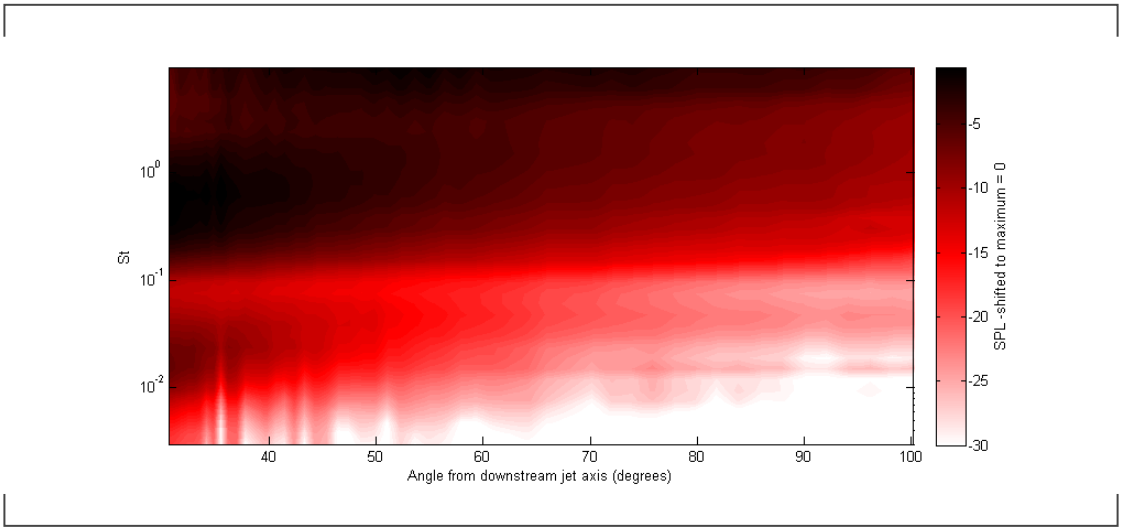

in density due to temperature differences. As these temperature differences are expected to be small this is acceptable and will only have a small effect on the accuracy of the Mach number calculation.

Results of Pipe Experiment

Analysis of sound measurements of the jet with resistance elements built into the pipe show that this does not alleviate the problem of the low frequency peak. Figures 6.18 and 6.19, for the M = 0.5 case show little significan difference to the experiments carried out without resistance elements in the pipe. (Compare to figure 6.9 and 6.10)

Unfortunately, the resistance elements built into the pipe cause additional problems. They generated a high frequency noise which was not present in the case without resistance elements and which, unlike the low frequency peak, is within the range of Strouhal numbers that are of significan interest for jet noise. Figures 6.20 to 6.23 show that this high frequency upstream noise causes serious problems in the measurement of jet noise at lower Mach numbers.

Figure 6.24 shows the JEXTRA data or the cases both with and without flo conditioning. The results match very closely, especially in the main range of interest, between Strouhal 0.1 and Strouhal 2. The lower frequency data shows slight discrepancy for the 90° case, but the general trend is very similar. At higher Strouhal numbers the high frequency disturbance due to the flo conditioning causes a significan difference in the

Abbildung 6.10.: **SPL versus Strouhal number for microphones at angles ~30° ~32.5° and 90°. For Lockheed data [9](left) and JEXTRA (02/09) data (right). M = 0.5 case**

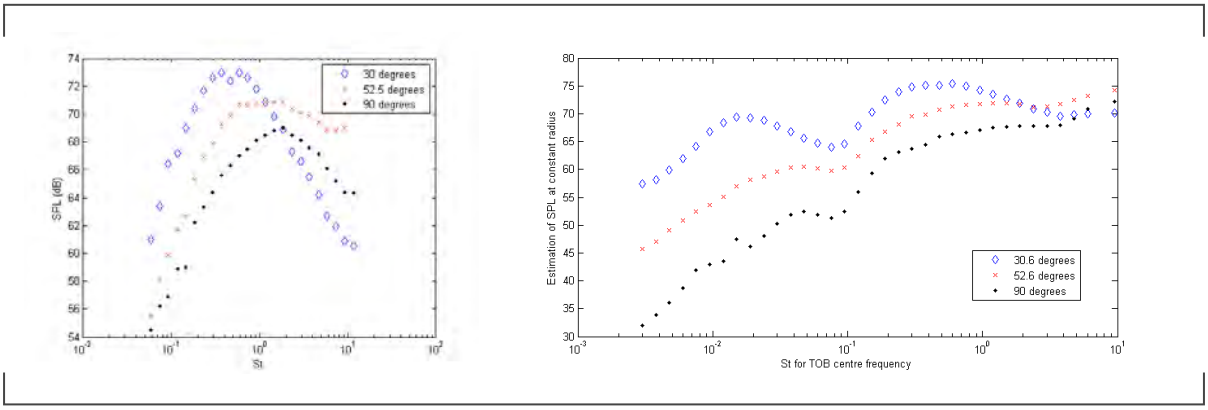

results between Strouhal 2 and Strouhal 3, which is a region that is still of significan interest for jet noise.

It can be concluded that the low frequency peak is unlikely to be due to pipe resonances as these would have been disturbed by the flo conditioning. The high frequency disturbance, probably caused by the chosen flo conditioning configuration has a negative impact on the range of frequencies over which useful results can be measured. The overall repeatability of the jet noise measurements on the rig have been shown to be good.

6.5.6. Mach Exponent Scaling

Dimensional Analysis

Dimensional analysis can be performed with the following variables:

Variable	Dimension	Description
Q_q	MLT^{-4}	source term
W_{qq}	$M^2\ L^{-2}\ T^{-7}$	cross spectral density of quadrupole source of strength Q_q
D_j	L	nozzle diameter
$\Delta U_j = U_j - U_f$	LT^{-1}	relative jet speed
ρ_∞	ML^{-3}	ambient density

The standard notation for the mass-distance-time set of dimensions (M for mass, L for distance, T for time) has been used [24].

Abbildung 6.11.: **SPL versus Strouhal number for microphones at angle ~30°. lockheed [9] and JEXTRA (02/09) data on same graph. M = 0.5 case.**

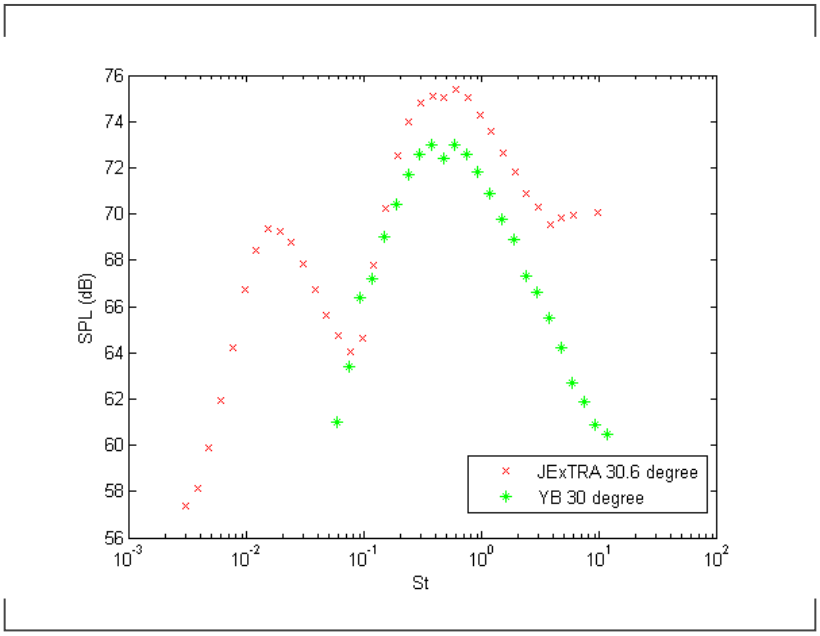

From these variables a scaling law for quadrupole sound sources can be derived. Similarly, scaling laws for monopole and dipole sources can also be derived. For the full derivations refer to the Aircraft Noise Course Lecture Script by Ulf Michel and Henri Siller [5].

It can be shown that monopole sound scales with M^4, dipole sound with M^6 and quadrupole sound with M^8.

By plotting $SPL - (n * 10)\log_{10} M$ versus Strouhal Number and identifying at which exponents the data for different Mach numbers collapses onto a single curve it should be possible to identify which parts of the spectrum come from which kind of source.

Note this is only valid at high Mach numbers, say above M=0.5, although the M=0.4 case may work too.

Physically, quadrupole sound is most commonly associated with the turbulent structures in the shear layer that generate jet noise [5]. Dipole noise is commonly due to flo interacting with a lip or surface [23].

Ultimately scaling will be at something like 7.8 suggesting a combination of different scaling. For modelling purposes only scaling with n=4,6,8 is of interest. NB if it was an external source there would also be scaling: compressor would be n=1 (as compressor noise probably scales with angular speed, which is roughly linearly related to Mach num-

Abbildung 6.12.: **SPL versus Strouhal number for microphones at angle ~52.5°. Lockheed [9] and JEXTRA (02/09) data on same graph. M = 0.5 case.**

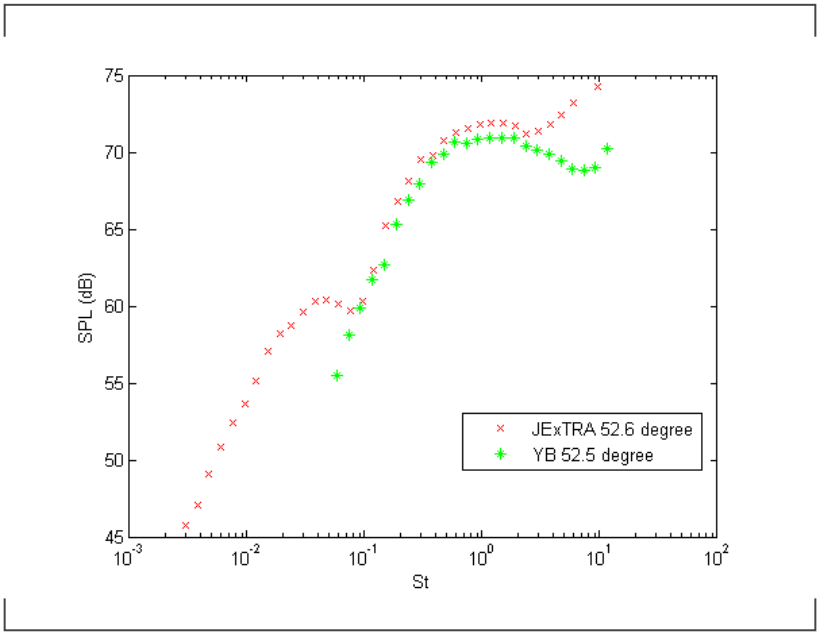

ber), if it was the power supply it is possible that scaling would be with n=2 i.e. the power required (kinetic energy scales with v^2).

Comparison data

Figure 6.25) shows the Lockheed data scaled with n=4, n=6 and n=8 to identify the Mach Number exponent that best characterises the data. Clearly n=8 gives the best collapse onto a single curve. The M=0.4 case does not collapse onto the curve with the other cases, which is explained by the fact that the scaling relation is only really valid at higher Mach numbers. M^8 collapse indicates quadrupole sound [6].

JEXTRA data

Figures 6.26 shows the data for the microphone at a polar angle of 90° to the jet axis for various Mach numbers plotted on the same axis as described above. By visual inspection, the points composing the high frequency peak seem to collapse onto a single curve best at n=8, while the points composing the low frequency peak collapse onto a single curve

Abbildung 6.13.: **SPL versus Strouhal number for microphones at angle 90°. Lockheed [9] and JEXTRA (02/09) data on same graph. M = 0.5 case.**

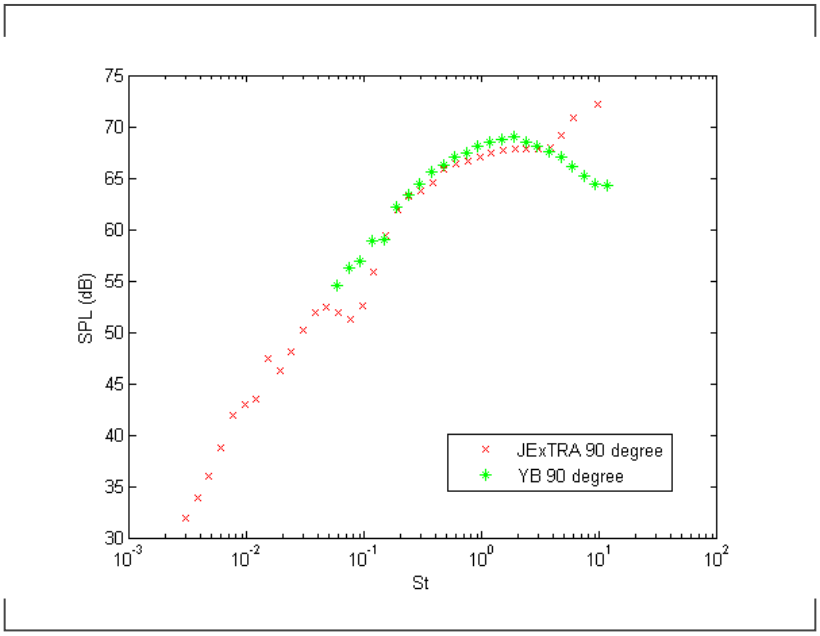

best at n=6.

The M^8 scaling matches the comparison data well over a similar range of Strouhal numbers and indicates quadrupole noise [6]. The M^6 scaling suggest dipole noise which could be accounted for by a lip or surface interaction [23].

Figure 6.27 shows zoomed in views of the regions of interest.

In order to validate or reject the hypothesis made about the low frequency peak found in the jet noise results, SODIX could be used to identify where the low frequency sources are. If the sources come from the jet this would support the evidence from scaling analysis presented in this section. This application of SODIX is highlighted as an area for further work on the project.

An additional area for further work on the scaling analysis results, could be to plot how the Mach exponent varies with frequency. This analysis could be carried out on the data already available.

6.5.7. Near Field Correction

As shown in figur 6.28, based on information in [5], different regions of the jet contain sound sources with different directivities and different frequencies. Small scale structures near the nozzle are responsible for high frequency sound with a high polar emission angle, while larger structures towards the end of the potential core are responsible for lower frequency sound, with a directivity that extends to much lower polar angles. This is represented schematically in figur 6.28.

When measuring in the far field each microphone will receive sound from sources with a similar directivity, and thus the directivity pattern of the entire jet can be analysed.

For microphones in the near field such as the one shown in figur 6.28, the situation is different. Microphones will 'see' different sources at very different angles, and the polar angle of a microphone with respect to the nozzle exit, can be very different from that with respect to low frequency sources. This effect is generally refered to as biasing.

To illustrate this consider the microphone at an observer angle of 90°. For a microphone in the far fiel this will measure the sound from all sources at a source directivity of very close to 90°. For a microphone in the near field sound from the high frequency sources near the nozzle will be at a source directivity of roughly 90°, but the low frequency sound measured (from sources further downstream) will have been emitted at higher polar angles. The same effect applies for all other microphone positions, which means that a direct comparison of near fiel and far fiel data is not possible.

Note that in the measurements conducted the closest microphone to the nozzle is only 11.6 nozzle diameters away, so the microphones are located in the geometric near field In comparison the Lockheed data [9] was taken at a distance of $R_{yb} = 78D$, which is in the far field

In order to be able to compare the results a near-fiel correction must be carried out for the measured data. There are two possible methods for this. The firs is to use a microphone to measure the frequency of sources within the jet itself. Knowledge of the source distribution can then be used to correct the data. Alternatively a SODIX source identificatio calculation can be carried out on the near fiel data, and the resulting source distribution used to calculate a far-fiel result. This SODIX simulation is recommended for future work on this project.

6.5.8. Inspection of Data from Ring Array

Figure 6.29 shows that all microphones on the ring give very similar values of SPL for the high frequency lobe, but that there is significan discrepancy for the low frequency lobe. In terms of Strouhal number, the Sound Pressure Level at the different microphones on the ring matches well in the region St = 0.1 – 3.0, which is the main area of interest for jet noise.

A possible cause for the discrepancy at high frequencies is scattering at the microphones. The high frequency waves have a very short wavelengths, so this could be a very localised effect.

The low frequency discrepancy could be related to standing waves set up in the room. This possibility could be investigated by traversing a microphone.

6.6. Discussion of Validity of Rig for Jet Noise Measurements

In the range of Strouhal numbers from St = 0.1 to St = 3 there is good agreement between the spectra measured on the Rig, and comparison data from experiments carried out by Lockheed [9].

The high frequency discrepancy could be due to effects of the set-up, such as scattering from the brass pipes of the microphone array or other effects.

The comparison data does not extend to low frequencies, but the second low frequency peak would not usually be expected in far-fiel jet noise spectra.

A Mach exponent scaling analysis showed that for Mach numbers above M = 0.5 the results in the range of Strouhal numbers from St = 0.1 to St = 3 collapse quite well onto

a single curve at n=8 for both the comparison data and the data from measurements on the JEXTRA rig, which is characteristic of sound from quadrupole sources. The low frequency results from the JEXTRA measurements collapse at n = 6, which suggests dipole sources. Dipole sources are often associated with flow-surfac interactions [23].

Inspection of results from measurements on a ring of microphones at a moderate polar angle show good consistency in the range of Strouhal numbers from St = 0.1 to St = 2. Below Strouhal 0.1 the pattern is the same for all microphone positions but the SPL varies.

Abbildung 6.14.: **Contour plots to show variation with Mach number. M = 0.3, 0.4, 0.5, 0.6 0.7 from top left to bottom.**

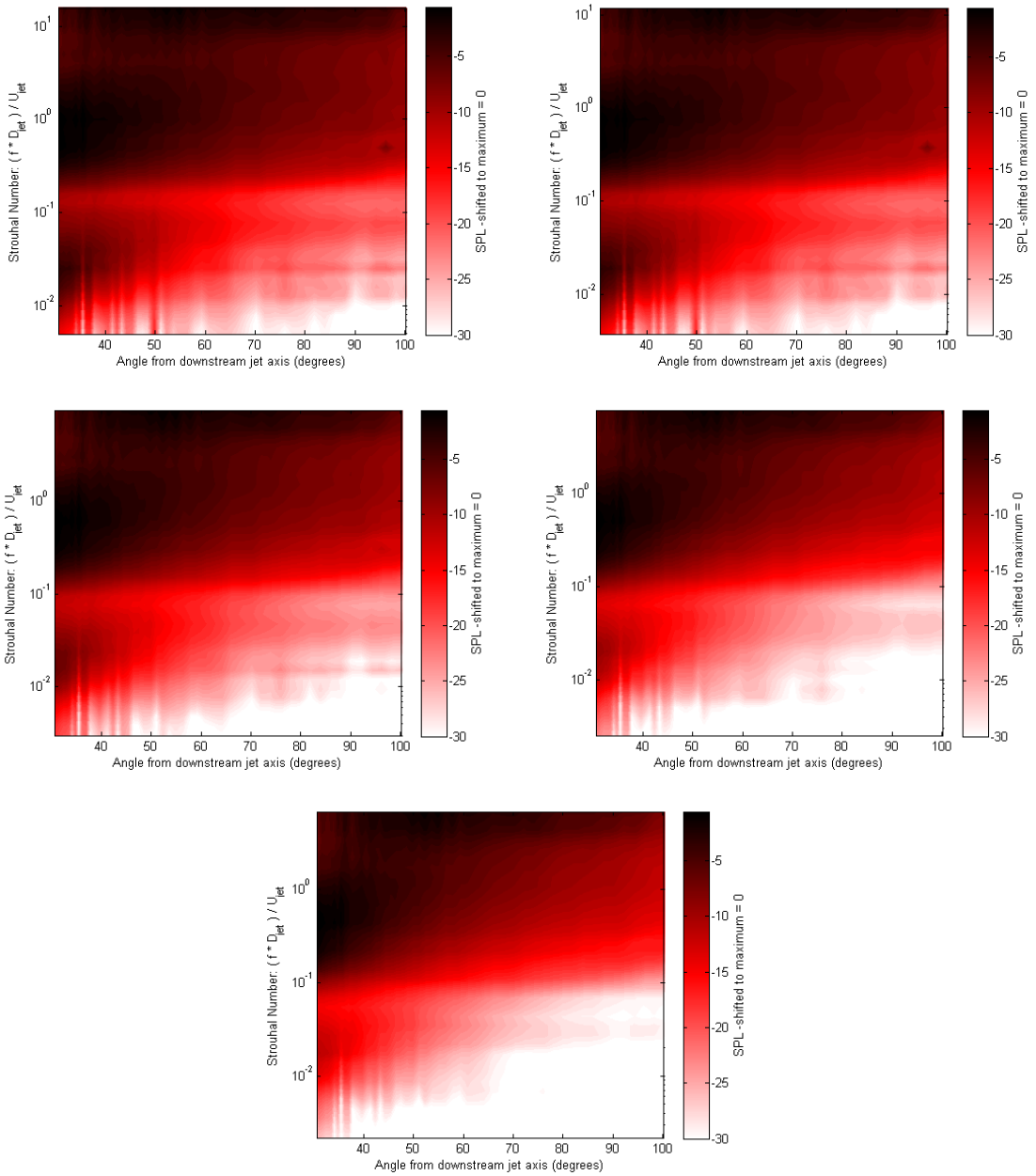

Abbildung 6.15.: **Sound Pressure Level versus Strouhal Number for microphone at polar angle of 90°. M = 0.3 – 0.7. JEXTRA data (02/09).**

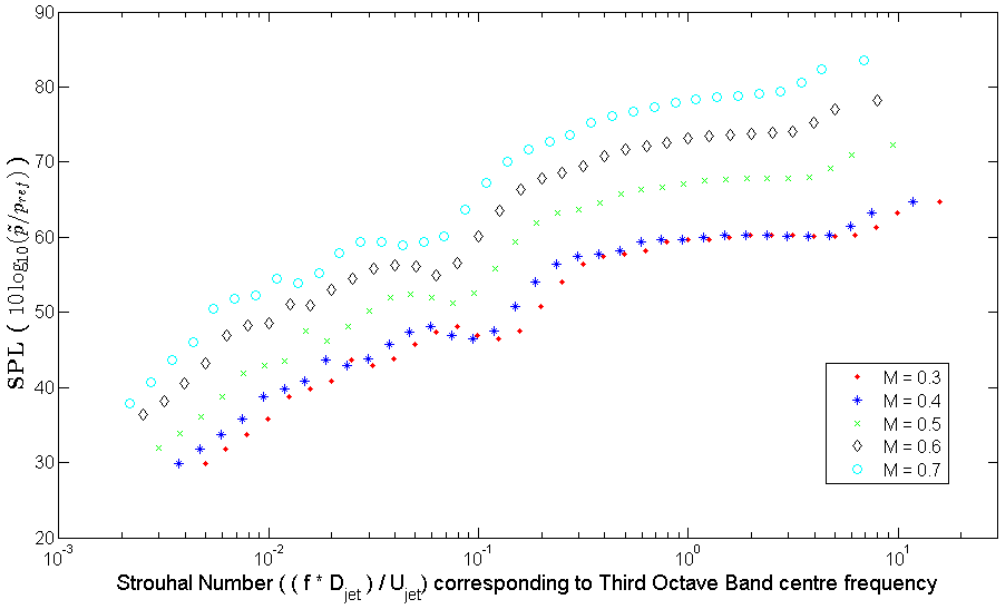

Abbildung 6.16.: **Photograph of perforated cone and honeycomb. [Wolfram Hage]**

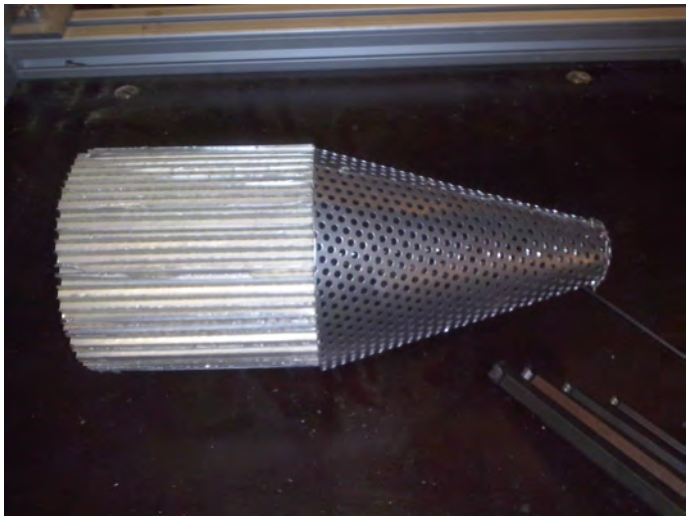

Abbildung 6.17.: **Photograph of perforated cone inserted into pipe. Taken 03/09/15 .**

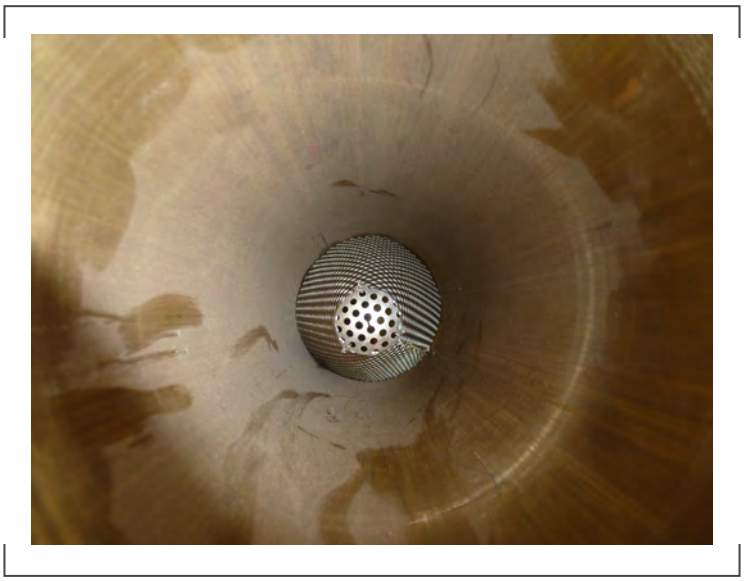

Abbildung 6.18.: **Case with resistance element (JEXTRA 03/09). Contour Map of SPL on an axis of Strouhal number versus Microphone Angle. M = 0.5 case.**

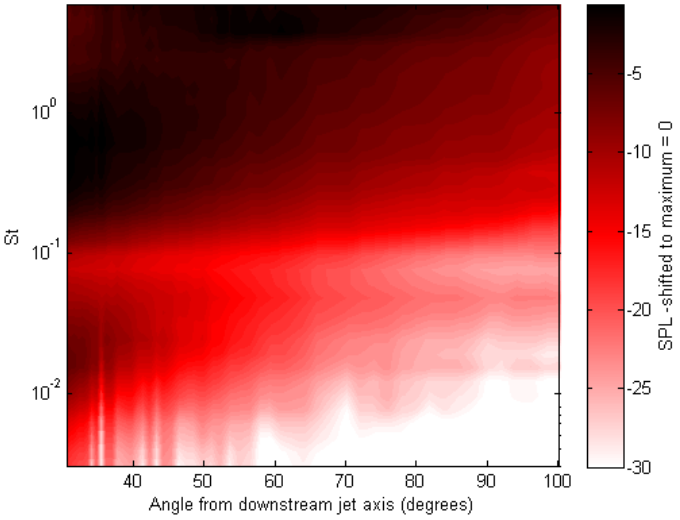

Abbildung 6.19.: **Case with resistance element (JEXTRA 03/09). SPL versus Strouhal number for different angles. M = 0.5 case.**

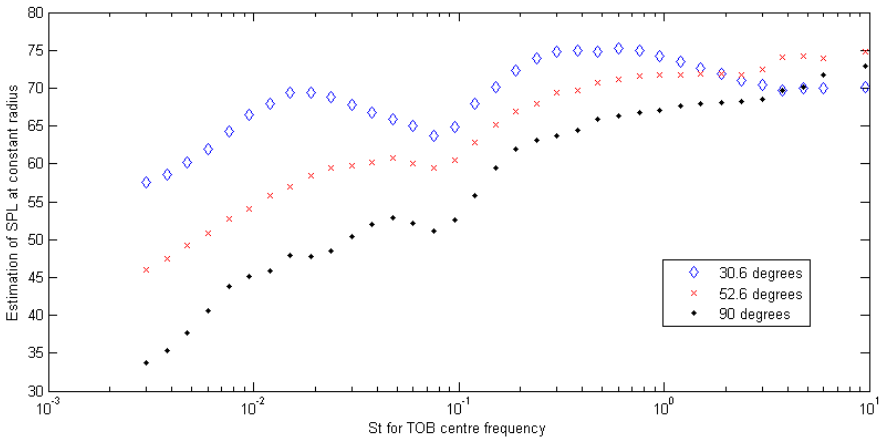

Abbildung 6.20.: **Case with resistance element (JEXTRA 03/09). Contour Map of SPL on an axis of Strouhal number versus Microphone Angle (left). Plot of SPL versus Strouhal number for different angles (right). M = 0.3 case.**

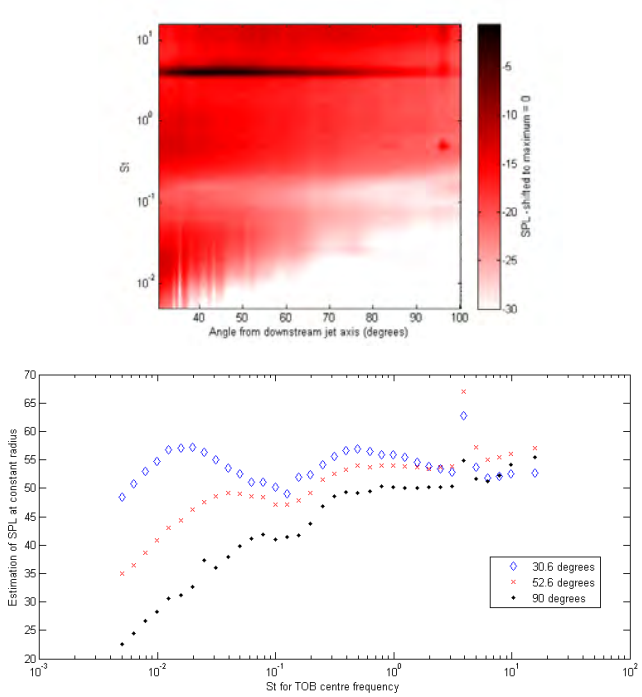

Abbildung 6.21.: **Case with resistance element (JEXTRA 03/09). Contour Map of SPL on an axis of Strouhal number versus Microphone Angle (left). Plot of SPL versus Strouhal number for different angles (right). M = 0.4 case.**

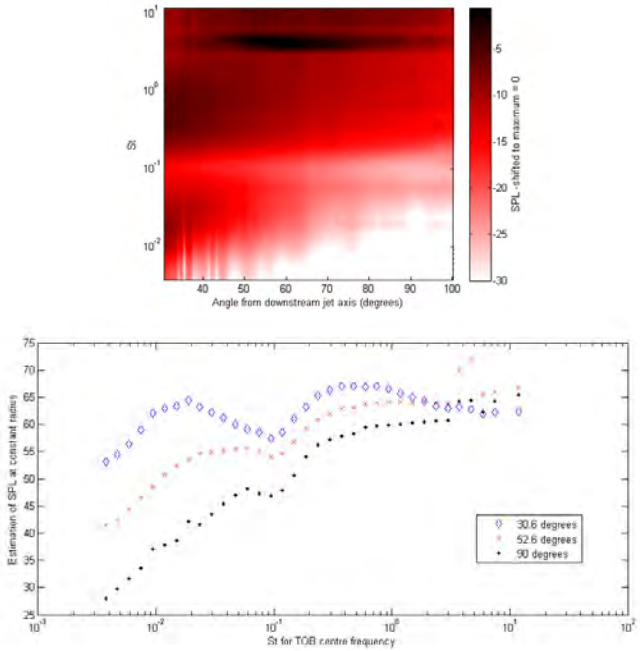

Abbildung 6.22.: **Case with resistance element (JEXTRA 03/09). Contour Map of SPL on an axis of Strouhal number versus Microphone Angle (left). Plot of SPL versus Strouhal number for different angles (right). M = 0.5 case.**

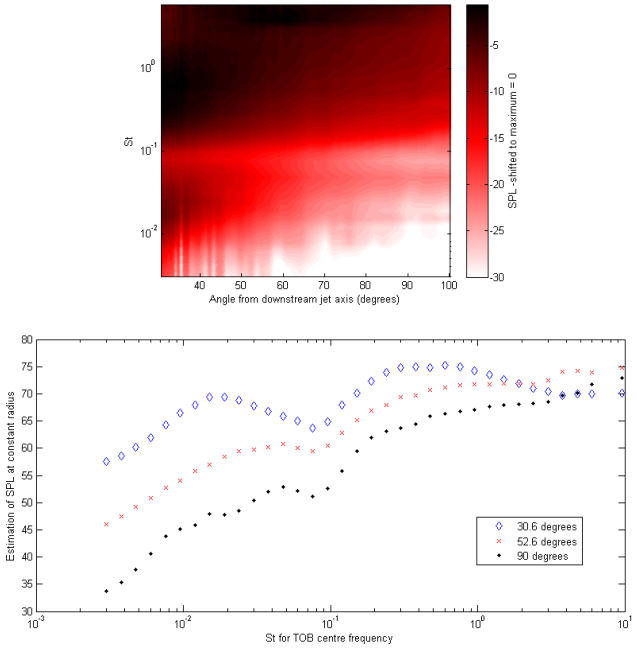

Abbildung 6.23.: **Case with resistance element (JEXTRA 03/09). Contour Map of SPL on an axis of Strouhal number versus Microphone Angle (left). Plot of SPL versus Strouhal number for different angles (right). M = 0.6 case.**

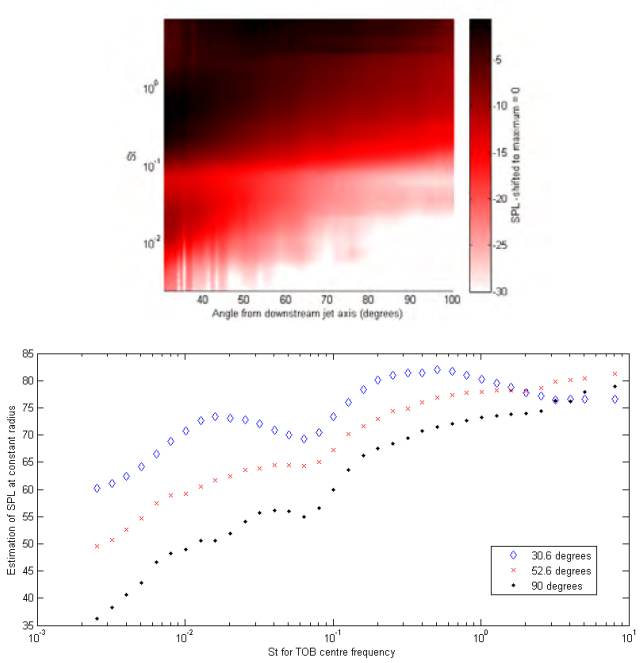

Abbildung 6.24.: **Estimation of SPL $10\log_{10}(\tilde{p}/p_{ref})$ at Constant Radius 3.9 m versus Strouhal Number for microphones at different angles. Results without flo conditioning shown in blue, results with f ow conditioning shown in red.**

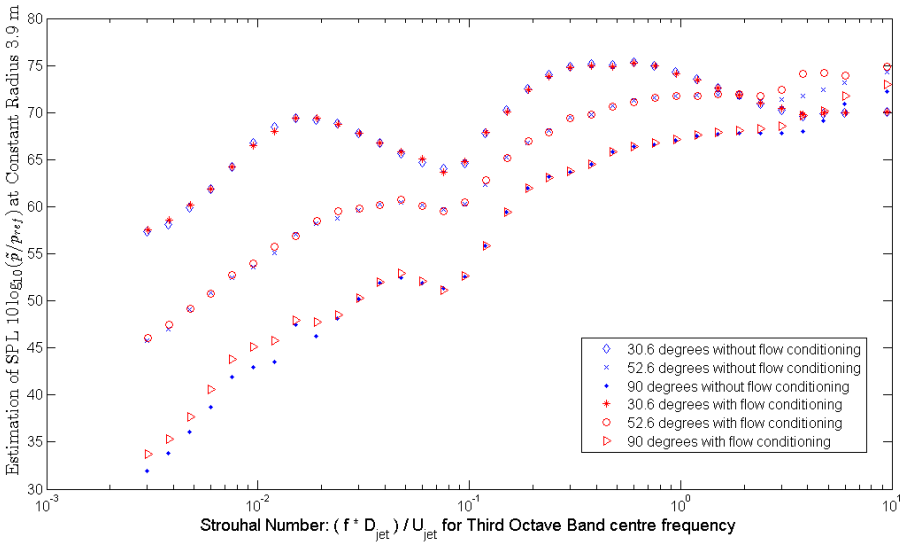

Abbildung 6.25.: **(SPL** $-(n*10)\log_{10}$ **(M)) versus Strouhal Number for values of n from 4 (top left) to 9 (bottom right). Lockheed data [9]. Third octave bands for microphone at 90°, over a range of Mach Numbers 0.4 - 0.7.**

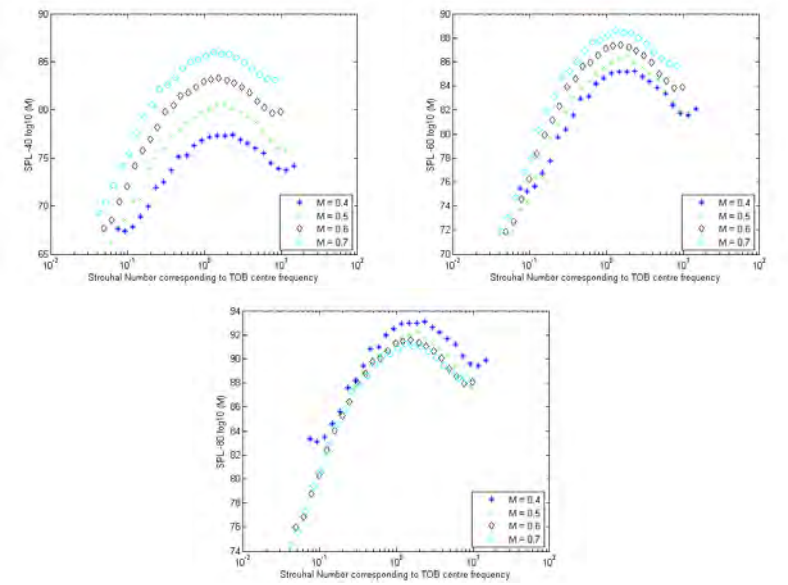

Abbildung 6.26.: **(SPL** $-(n*10)\log_{10}$ **(M)) versus Strouhal Number for values of n = 4, 6, 8 (left to right). JEXTRA data for case without resistance element (day 02/09). Third octave bands for microphone at 90°, over a range of Mach Numbers 0.4 - 0.7.**

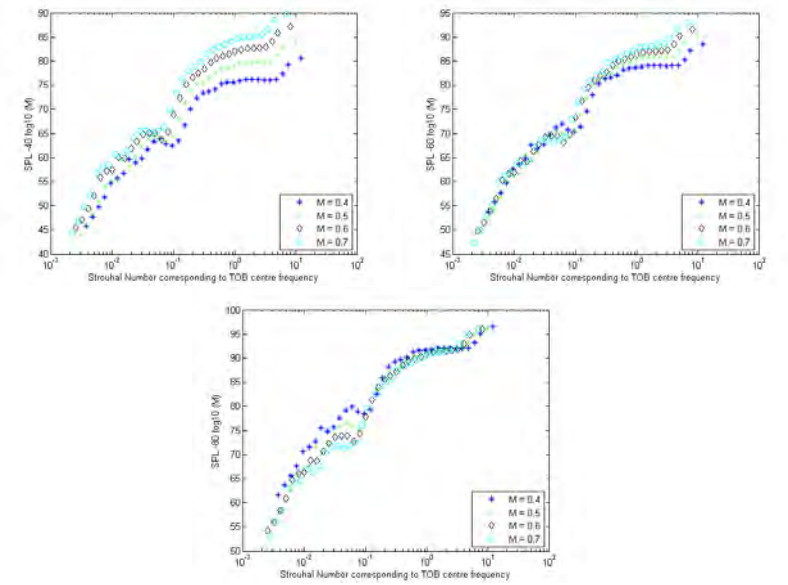

Abbildung 6.27.: **(SPL $-(n*10)\log_{10}(\mathrm{M})$) versus Strouhal Number for values of n = 6 (left) showing only the low frequency lobe, and n = 8 (right) showing only the high frequency lobe. JEXTRA data for case without resistance element (day 02/09). Third octave bands for microphone at 90°, for a range of Mach numbers 0.4 - 0.7.**

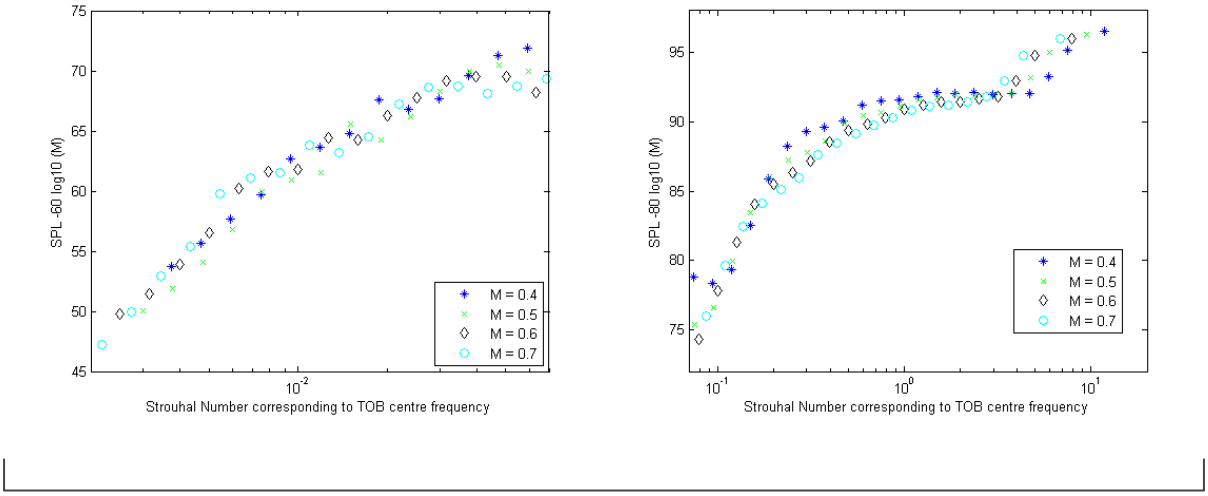

Abbildung 6.28.: **Sketch of sound source regions in a typical jet.**

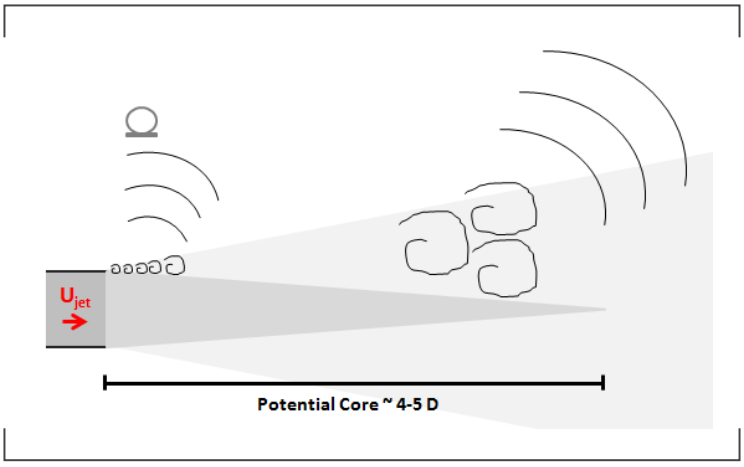

Abbildung 6.29.: **SPL versus St for all positions on the ring array. JEXTRA data (day 02/09) M = 0.5 case.**

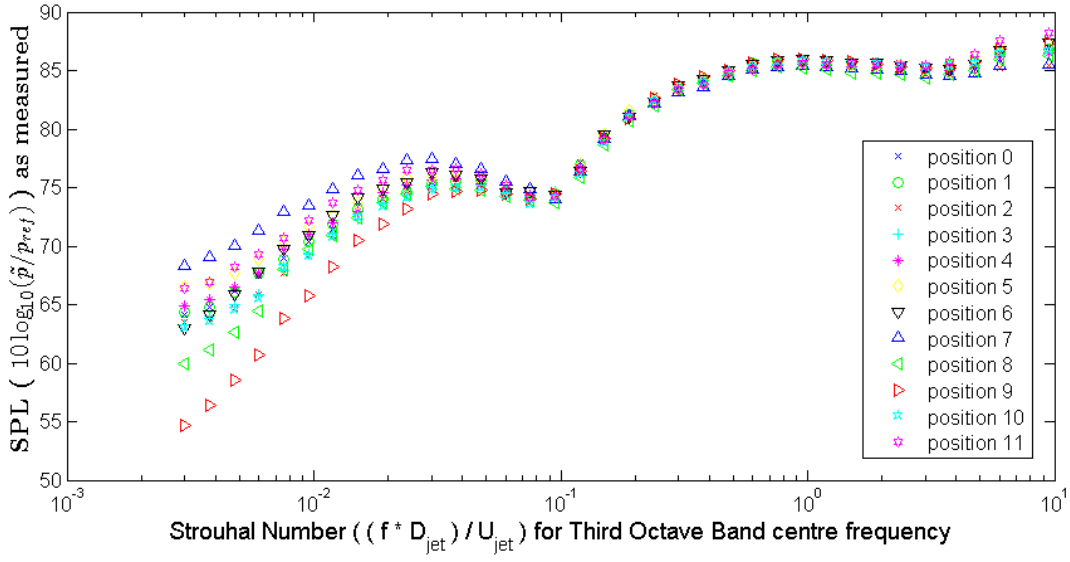

7. Future Work

Single Sound Source tests in the room without the 'anechoic' channel in place, to enable a quantitative comparative assessment of the effectiveness of the low-reflectio construction.

Extension of the linear array to lower polar angles (i.e. more microphones in the downstream direction). It would be interesting to see at what downstream angle a peak is reached. Eventually there should be a cone of relative silence. The aluminium holder on anechoic channel segment C already has further positions in the downstream direction. These simply have to be fille with brass pipes and microphones, following the protocol in section 3.4.

Analysis of coherence for the measurements on the microphone ring.

Application of SODIX for source identificatio of the sources contributing to the low frequency peak, in order to confirm/rejec whether this peak is directly related to the jet.

Application of SODIX to all jet data for source identification

Experiments with a different nozzle. A smaller nozzle will require the bypass to be in operation.

Near fiel correction of data using results from SODIX. Comparison of corrected data with original data.

Literaturverzeichnis

[1] *McCowan, I.* 'A Microphone Array Tutorial' *2004.*

[2] *McCowan, I.* 'Microphone Arrays: A Tutorial' *2001.*

[3] *Sinayoko, S. Agarwal, A.* 'Flow decomposition and aerodynamic sound generation' *Journal of Fluid Mechanics February 2011.*

[4] *Dowling, A. Ffowcs Williams, J.E.* 'Sound and Sources of Sound' *Ellis Horwood Limited 1983.*

[5] *Ulf, M. Siller, H.* 'Lecture Script: Aircraft Noise Course'

[6] *Suzuki, T.* 'A review of diagnostic studies on jet-noise sources and generation mechanisms of subsonically convecting jets' *Fluid Dynamics Research 2010.*

[7] *Fisher, M. J. et al.* 'A Modelling of the Noise from Simple Coaxial Jets, Part I: With Unheated Primary Flow' *Journal of Sound and Vibration 1998.*

[8] *Michalke, A. Fuchs, H. V.* 'On turbulence and noise of an axisymmetric shear flow *J. Fluid Mech. 1975.*

[9] *Tanna, H.K.* 'The Generation and Radiation of Supersonic Jet Noise. Volume III, Turbulent Mixing Noise Data' *Lockheed-Georgia Company 1976.*

[10] *Xiang, N. et al.* 'Experimental validation of a coprime linear microphone array for high-resolution direction-of-arrival measurements' *JASA Express Letters 2015.*

[11] *Karabasov, S. A.* 'Understanding jet noise' *Philosophical Transactions of The Royal Society 2010.*

[12] *Ouellette, N. T.* 'On the dynamical role of coherent structures in turbulence' *C. R. Physique 2012.*

[13] *Gramer, L.* 'Kelvin-Helmholtz Instabilities' *GFD-II 2007.*

[14] *Funke, S. et al.* 'SODIX in comparison with various deconvolution methods' *Berlin Beamforming Conference 2014.*

[15] *Michel, U. Funke, S.* 'New Source Analysis of an Aeroengine with a new Inverse Method SODIX' *14th AIAA/CEAS Aeroacoustics Conference 2008.*

[16] *Michel, U. Funke, S.* 'Inverse Method for the Acoustic Source Analysis of an Aeroengine' *Berlin Beamforming Conference 2008.*

[17] *Funke, S. et al.* 'An extended formulation of the SODIX method with application to aeroengine broadband noise' *18th AIAA/CEAS Aeroacoustics Conference 2012.*

[18] *Viswanathan, K. et al.* 'The sources of jet noise: experimental evidence' *J. Fluid Mech. 2008.*

[19] *Doebler, D. et al.* Automatic Detection of Microphone Coordinates *Berlin Beamforming Conference 2010.*

[20] *Bechert, D. W. Pfizenmaie , E.* Amplificatio of Jet Noise by Higher-Mode Acoustical Excitation *AIAA Journal CHECK from vol 15 no9. -1977?*

[21] *Doebler, D. et al.* Coherent Structures in Jet Turbulence and Noise *AIAA Journal 1977*

[22] *WRITE UP SOURCE PROPERLY.*
(The power point about the snowflak measurement system.)

[23] *N. Curle* The Influenc of Solid Boundaries upon Aerodynamic Sound *Proceedings of the Royal Society of London 1955*

[24] *Barenblatt, G. I.* Scaling *Cambridge Texts in Applied Mathematics 2003*

Appendices

A. Linear Array Strouhal Calculations

For reference, the frequencies that can be expected at different Strouhal and Mach numbers for the experimental set-up are shown here. The Strouhal number (St) is the dimensionless frequency of a static jet. It is given by:

$$St = \frac{f_s D_j}{U_j}$$

where f_s = frequency, D_j is the jet diameter, and U_j is the jet speed.

For the tests being carried out, the Mach number at nozzle exit is specified This can be used to calculate the jet velocity U_j:

$$U_j = M_j * a_j$$

Where a_j is the speed of sound in the jet, this will be slightly higher than the speed of sound in the free stream, as the jet is slightly hotter than the free stream. Assuming a jet temperature of around 40 °C, a_j is given by:

$$a_j = \sqrt{\gamma * R * T_{jet}}$$

$$a_j = \sqrt{1.4 * 287 * (40 + 273.15)} = 355 \; m/s$$

giving:

$$U_j = 355 * M_j$$

Rearranging the definitio of the Strouhal number to give an equation for the frequency, and subbing in the definitio of U_J gives:

$$f_s = St * 355 * M_j / D_j$$

Figure A.1 gives frequencies relating to different Strouhal numbers (St) and jet Mach numbers (M_j), assuming a jet diameter (D_j) of 50mm:

Abbildung A.1.: **Graph to show frequency versus Mach Number for a range of Strouhal numbers, for a diameter of 0.05m and a temperature of 40 °C.**

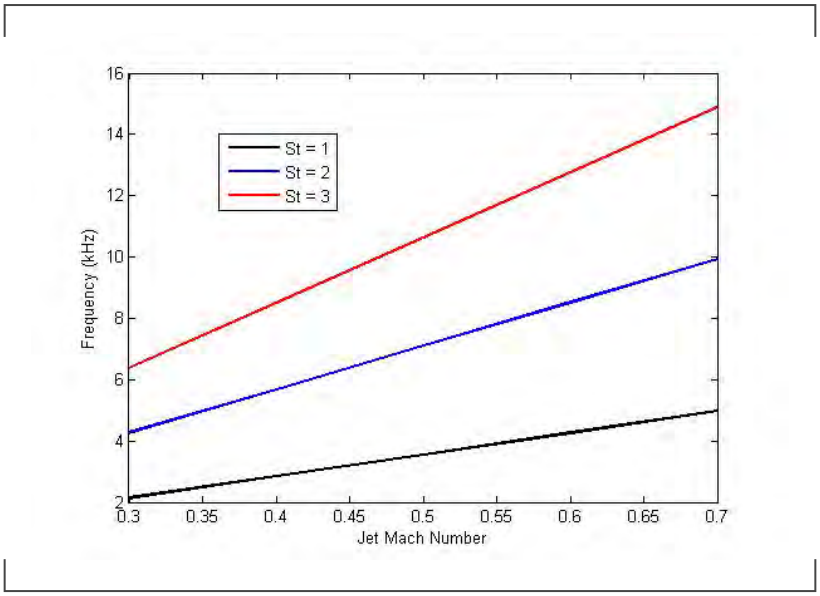

If $St = 1$ and $St = 2$ are the main areas of interest, then even for $M_j = 0.7$ the frequency does not exceed 10 kHz.

B. Jet Noise Tables

All the data and scripts (Python 3 and MATLAB) used to generate the graphical content of this report is stored in electronic form on the JEXTRA hard drive.

Jet Noise Tables in the format of the Lockheed data [9] can be generated from the stored data for SPLs, polar angles and frequencies if required, or by re-analysing the data from scratch if preferred.

C. Experimental log sheets

For the experiential log sheets please refer to the physical JEXTRA folder.

Some log-sheets have been typed up and can thus also be found in electronic form on the JEXTRA hard drive.

All log-sheets are clearly labelled with the date on which the experiments that they document were performed on, as is all the measurement data stored on the hard drive. README file are included to aid navigation through the data on the hard drive.

At time of writing a further electronic version exists under:
/home/terra/Transfer/Bassetti/JEXTRA/

D. Determination of Microphone Positions

For all data analysis in this report, nominal microphone positions have been used. As discussed in the report, the true microphone positions will deviate from these nominal values.

The determination of microphone positions was a topic of discussion throughout the project, but at the time of writing no suitable method had been agreed upon.

Methods similar to the one described in source [19], were considered, but rough calculations suggest that the accuracy of this method will be insufficie t, especially when the maximum sampling frequency of the snowflak system is taken into account.

The identificatio or development of a technique to accurately determine microphone positions is an important area for future work on the project. The application of SODIX in particular would benefi from more accurate knowledge of microphone coordinates.